



Combined U–Pb, Lu–Hf, Sm–Nd and Ar–Ar multichronometric dating on the Bailang eclogite constrains the closure timing of the Paleo-Tethys Ocean in the Lhasa terrane, Tibet



Hao Cheng^{a,*}, Yumeng Liu^a, Jeffrey D. Vervoort^b, Honghua Lu^c

^a State Key Laboratory of Marine Geology, Tongji University, Shanghai 200092, China

^b School of the Environment, Washington State University, Pullman, WA 99164, USA

^c School of Resources and Environment Science, East China Normal University, Shanghai 200062, China

ARTICLE INFO

Article history:

Received 23 June 2014

Received in revised form 25 September 2014

Accepted 28 September 2014

Available online 30 October 2014

Handling Editor: Z.M. Zhang

Keywords:

Lhasa terrane

Tibet

Eclogite

Lu–Hf

Subduction

ABSTRACT

The Lhasa terrane, the main tectonic component of the Himalayan–Tibetan orogen, has received much attention as it records the entire history of the orogeny. The occurrence of Permian to Triassic high-pressure eclogites has a significant bearing on the understanding of the Paleo-Tethys subduction and plate suturing processes in this area. An eclogite from the Bailang, eastern Lhasa terrane, was investigated with a combined metamorphic *P–T* and U–Pb, Lu–Hf, Sm–Nd and Ar–Ar multichronometric approach. Pseudosection modeling combined with thermobarometric calculations indicate that the Bailang eclogite equilibrated at peak *P–T* conditions of ~2.6 GPa and 465–503 °C, which is much lower than those of Sumdo and Jilang eclogites in this area. Garnet–whole rock–omphacite Lu–Hf and Sm–Nd ages of 238.1 ± 3.6 Ma and 230.0 ± 4.7 Ma were obtained on the same sample, which are largely consistent with the corresponding U–Pb age of 227.4 ± 6.4 Ma for the metamorphic zircons within uncertainty. The peak metamorphic temperature of the sample is lower than the Lu–Hf and Sm–Nd closure temperatures in garnet. This, combined with the core-to-rim decrease in Mn and HREE concentrations, the slightly U-shaped Sm zonation across garnet and the exclusive occurrence of omphacite inclusion in garnet rim, are consistent with the Lu–Hf system skewing to the age of the garnet core and the Sm–Nd system favoring the rim age. The Sm–Nd age was thus interpreted as the age of eclogite-facies metamorphism and the Lu–Hf age likely pre-dated the eclogite-facies metamorphism. ⁴⁰Ar/³⁹Ar dating of hornblende from the eclogite yielded ages about 200 Ma, which is interpreted as a cooling age and is probably indicative of the time of exhumation to the middle crust. The difference of peak eclogite-facies metamorphic conditions and the distinct metamorphic ages for the Bailang eclogite (~2.6 GPa and ~480 °C; *ca.* 230 Ma), the Sumdo eclogite (~3.4 GPa and ~650 °C; *ca.* 262 Ma) and Jiang eclogite (~3.6 GPa and ~750 °C; *ca.* 261 Ma) in the same (ultra)-high-pressure belt indicate that this region likely comprises different slices that had distinct *P–T* histories and underwent (U)HP metamorphism at different times. The initiation of the opening the Paleo-Tethys Ocean in the Lhasa terrane could trace back to the early Permian. The ultimate closure of the Paleo-Tethys Ocean in the Lhasa terrane was no earlier than *ca.* 230 Ma.

© 2014 International Association for Gondwana Research. Published by Elsevier B.V. All rights reserved.

1. Introduction

The Tibetan plateau, Earth's largest ongoing continent–continent collisional orogen, has been the focus of many recent scientific investigations. Closure of the Tethys Ocean, which separated the two continents, involved accretion of multiple intra-oceanic arcs and microcontinents, before culminating in continent–continent collision (Yin and Harrison, 2000). Several high-pressure metamorphic terranes, such as Amdo (Zhang et al., 2013), Qiangtang (Metcalfe, 1996; Zhu et al., 2013) and Lhasa terrane (Yang et al., 2009; Chen et al., 2013; Zhang et al., 2014a; Z.M. Zhang et al., 2014b), have been formed before the

final collision of the India and Eurasian plates between 40 and 50 Ma. Recently, a number of studies from various aspects, such as magmatism (e.g., Zhang et al., 2012; Ding et al., 2015; Hébert et al., 2014), geophysics (e.g., Chen et al., 2013; Xu et al., 2015; Zhao et al., 2014), paleomagnetism (e.g., Ran et al., 2012; Sun et al., 2012; Klootwijk, 2013), petrology and geochemistry (e.g., Li et al., 2011; Hébert et al., 2012; Liu et al., 2015), sedimentary and paleogeography (e.g., Zhu et al., 2011; Zhang et al., 2013; Li et al., 2014) and metamorphism (e.g., Yang et al., 2009; Cheng et al., 2012), have improved our understanding of the evolution of this giant orogen (cf. Zhang et al., 2012; Zhang et al., 2014a; Zhang et al., 2014b).

Due to its large size, high elevation, and remoteness, however, there are significant gaps in our understanding on the geology of the Tibetan plateau, particularly within its interior. For example, the geological

* Corresponding author. Tel./fax: +86 21 65985251.
E-mail address: oahgnehc@gmail.com (H. Cheng).

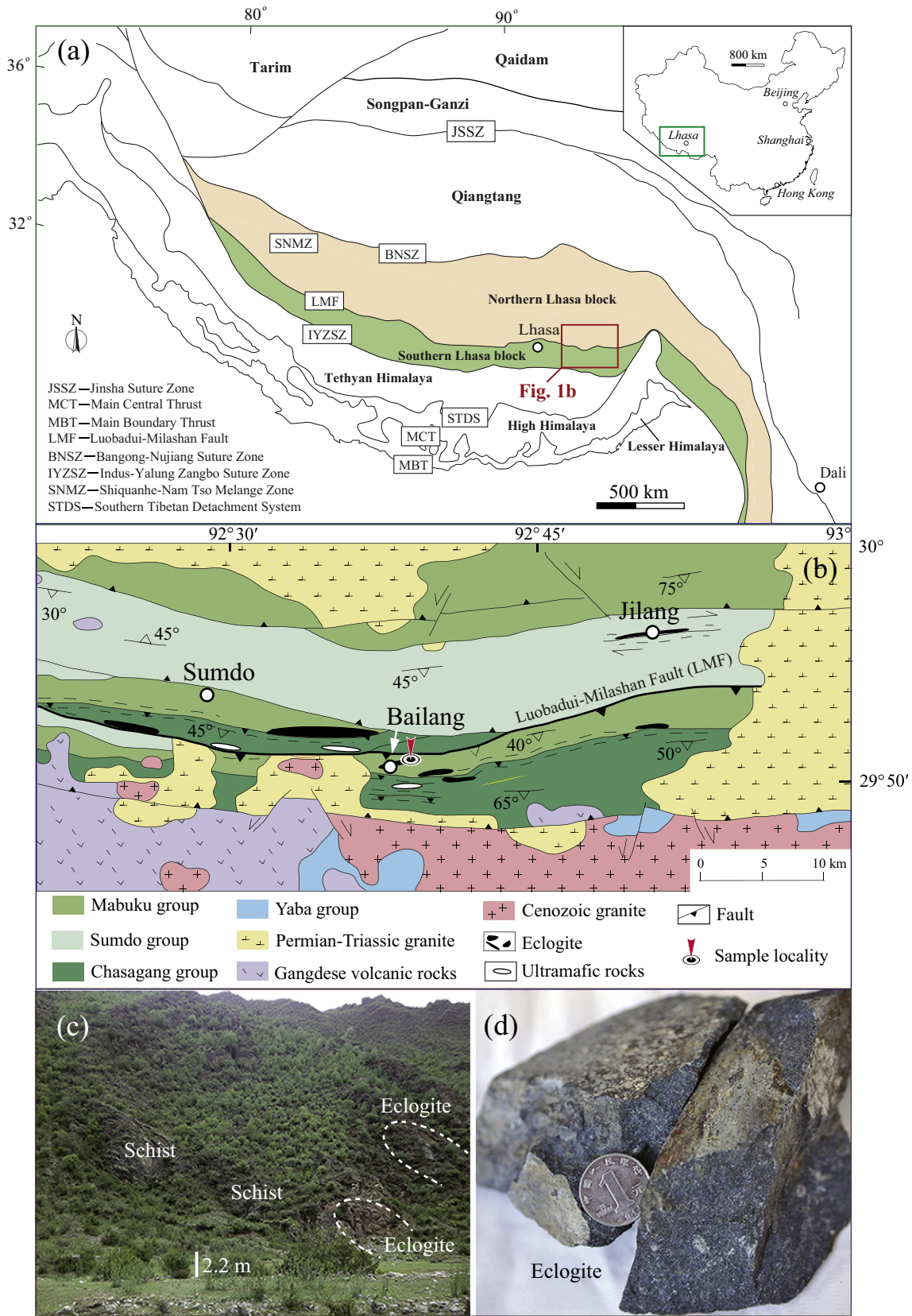


Fig. 1. (a) Schematic geological map of the Tibetan Plateau. (b) Geological map of the Bailang eclogite, showing the localities of Sumdo, Jilang and Bailang eclogites; compiled from maps by Yang et al. (2009), Li et al. (2011) and Cheng et al. (2012), and our own field observations. (c–d) Field occurrence of the Bailang eclogite.

evolution of these terranes prior to their accretion to Asia is not well known (Gynn et al., 2012). The Lhasa terrane, located in the southern part of Tibet, is a large crustal segment with a width of 100–300 km and

a length of around 2000 km (Fig. 1). The Lhasa terrane is composed of Precambrian crystalline basement, Paleozoic to Mesozoic sedimentary strata and Paleozoic to Cenozoic magmatic rocks (Zhang et al., 2014a;

Zhang et al., 2014b). This terrane was speculated to have rifted from Gondwana in the Triassic or the Middle to Late Jurassic and drifted northward across the Tethyan Ocean basins before it collided with Eurasia along the Bangong–Nujiang suture in the Cretaceous (Zhu et al., 2011, 2013). The Lhasa terrane is thus essential for revealing the origin and evolutionary history of the Himalayan–Tibetan orogen. The Lhasa terrane is bounded to the north by the Banggong–Nujiang Suture and to the south by the Indus–Yarlung–Tsangpo Suture (Fig. 1a). The identification of the Sumdo eclogite with typical N-MORB geochemical signatures and the association of ultramafic rocks to the south of the Sumdo eclogite belt (Yang et al., 2009) appear to suggest that the Lhasa terrane consisted of a North Lhasa segment and a South Lhasa segment separated by a Paleo-Tethys Ocean prior to the Late Paleozoic. Unraveling the metamorphic history of the Lhasa terrane, especially the eclogites, is necessary to answer the unresolved questions, such as when the subduction initiated and the timing of the final closure of the Paleo-Tethys Ocean, and may allow us to place critical limits on the reconstruction of the geodynamic evolution of the Himalayan–Tibetan orogen and the Tethys. Published U–Pb zircon and garnet Sm–Nd and Lu–Hf ages from the Sumdo and Jilang eclogites span over 65 Myr and do not provide the necessary constraints on the metamorphic history of the Lhasa terrane. These include: two Sm–Nd ages of $(306 \pm 50 \text{ Ma, Li et al., 2009; } 239.0 \pm 3.5 \text{ Ma, Zeng et al., 2009})$ and a weighted mean zircon U–Pb age of $262 \pm 5 \text{ Ma (Yang et al., 2009)}$ for the Sumdo eclogite, and a Lu–Hf age of $265.9 \pm 1.1 \text{ Ma}$ and two zircon age populations of *ca.* 261 Ma and *ca.* 238 (Cheng et al., 2012) for the Jilang eclogite.

In this paper we present U–Pb, Lu–Hf, Sm–Nd and Ar–Ar data for the Bailang eclogite in the Lhasa terrane (Fig. 1b–d). Our new Triassic ages differ from the existing geochronological data for the Sumdo and Jilang eclogites in this area. The diverse ages likely suggest the Lhasa terrane comprised different slices that recorded different metamorphic histories, reflecting distinct subduction and exhumation processes. These ages also imply that the final closure of the Paleo-Tethys Ocean in the Lhasa terrane was no earlier than *ca.* 230 Ma.

2. Geological outline and sample descriptions

The ancient Tethys oceanic realm in Asia is subdivided into three parts (Sengör, 1984; Metcalfe, 1996): the Paleo-Tethys, which separated the Cimmerian terranes (including the Qiangtang and Sibumasu terranes) from Eurasia; the Meso-Tethys, which separated the Lhasa and Qiangtang terranes (Fig. 1); and the Neo-Tethys, which was consumed between India and the southern margin of Eurasia. These three designations have been interpreted to belong to one oceanic lithosphere that was created and consumed between distinct continental terranes, rather than indicating separate and unconnected oceans (Guynn et al., 2012).

The Lhasa and Qiangtang terranes are interpreted to have been located along East Gondwana's margin during the Paleozoic on the basis of widespread Carboniferous–Permian diamictites and Gondwana flora and fauna (Leeder et al., 1988; Metcalfe, 1996). Ferrari et al. (2008) proposed that the Lhasa terrane was located next to northwest Australia during the Late Carboniferous based on their suggestion of southward subduction of the eastern Paleo-Tethys and a reinterpretation of northern Lhasa terrane Permian volcanic rocks as arc-related rather than rift-related. Zhu et al. (2011) suggested that during the Late Carboniferous to Early Permian the northern Lhasa terrane was located at north of Gondwana within the Paleo-Tethys Ocean. According to this model, the southern Paleo-Tethys ocean subducted northward beneath the Lhasa terrane's southern margin leading to collision of the Lhasa terrane with northwest Australia during the Late Permian.

The Lhasa terrane is bounded to the north by the Banggong–Nujiang Suture (Meso-Tethys) and to the south by the Indus–Yarlung–Tsangpo Suture (Meso-Tethys) (Fig. 1a). The Bangong–Nujiang suture zone (BNSZ), which extends for more than 2000 km across the central Tibetan Plateau, marks the site where the Bangong–Nujiang Tethyan Ocean

lithosphere was subducted either northward under the Qiangtang terrane during the Mesozoic (Coulon et al., 1986; Yin and Harrison, 2000) or southward under the Lhasa terrane during the Permian – Early Cretaceous (Hsü et al., 1995; Zhu et al., 2011). The Indus–Yarlung Zangbo suture zone (IYZSZ), which extends, for more than 2000 km from NW India via southern Tibet to NE India, is bounded to the north by the Xigaze forearc basin sequence and the Gangdese batholith and to the south by a Triassic flysch. It marks the site where the Indus–Yarlung Zangbo Tethyan Ocean lithosphere was consumed at a subduction zone dipping northward beneath the Lhasa terrane (Sengör, 1984; Girardeau et al., 1985; Yin and Harrison, 2000).

The Luobadui–Milashan Fault (LMF) is a large thrust fault, extending for ~1500 km across the southern part of the Lhasa terrane (Yang et al., 2009). Yang et al. (2009) identified a 500–1000-m-wide eclogite belt stretching for more than 100 km around the Sumdo area along the LMF. Peridotites are spatially associated with the Sumdo eclogite belt (BGMRXAR, 1993; Chen et al., 2009) and are in fault contact with a micaschist to the north and with greenschist rocks to the south. Zircons from lava within the greenschist have a U–Pb age of *ca.* 305 Ma, which is interpreted as the formation age of the greenschist (Chen et al., 2009), suggesting they are coeval with the Sumdo eclogite protoliths. Liu et al. (2009b) reported the presence of garnet glaucophane blueschists in association with Permian limestone and quartzite from Pangna, ~80 km west of the Sumdo. *P–T* calculations indicate that the Pangna blueschists experienced eclogite-facies metamorphism at conditions similar to those of the Sumdo eclogite in the same tectonic environment (Liu et al., 2009b).

Metamorphic rocks, which crop out in the east-central region of the Lhasa terrane, consist of eclogite, greenschist, marble, mica schist, and quartzite (Yang et al., 2006). The eclogite occurs as layers and lenses in the host schist, greenschist or quartzite. Previous studies are limited to two eclogite outcrops (Sumdo and Jilang, Fig. 1b). The Sumdo eclogite was estimated to have formed at 2.7 GPa and 730 °C (Yang et al., 2009). However, a recent study shows that the Sumdo eclogite may equilibrated at 760–800 °C and 3.3–3.9 GPa (Zhang et al., 2011). The Jilang eclogite is estimated to have formed at 3.4–3.8 GPa and 753–790 °C (Cheng et al., 2012). Quartz inclusions in omphacite and garnet showing expansion fractures surrounding them, a feature typical of quartz pseudomorphs after coesite, have been observed in both the Sumdo (Yang et al., 2006; Zhang et al., 2011) and Jilang eclogites (Cheng et al., 2012). Thus, we regard that both the Sumdo and Jilang eclogites experienced ultra-high-pressure (UHP) metamorphism. The timing of the eclogite-facies metamorphism has been constrained to be Late Permian based on Lu–Hf isochron dating of the Jilang eclogite (Cheng et al., 2012) and zircon U–Pb dating of the Sumdo and Jilang eclogites (Yang et al., 2009; Cheng et al., 2012).

The eclogite samples examined in this study were sampled at the Bailang (sample BLa-i; 29°54'N, 92°30'E, 4194 m), approximately 180 km east of Lhasa City. The eclogite bodies with variable size (1–20 m in diameter) occur in the mica-quartz schist (Fig. 1c). The Bailang eclogite is massive and dark blue (Fig. 1d). Of 9 samples for bulk geochemical analysis, one of the fresh samples was chosen for further petrological and geochronological investigations.

3. Analytical procedures

Major and trace-element chemical compositions of whole-rock powders were obtained by XRF and ICP-MS at Washington State University. Analytical procedures have been described by Cheng et al. (2011).

Mineral analyses were performed by electron microprobe (JEOL JXA 8100) at the China University of Geosciences in Wuhan. A 2 µm defocused beam was used at an acceleration voltage of 12 kV with a beam current of 20 nA.

Mineral inclusions in zircon were identified by a Renishaw RM 2000 Raman spectrometer at CAS Key Laboratory of Crust–Mantle Materials

and Environments in University of Science and Technology of China, Hefei. Garnet and zircon trace element abundances were measured LA-ICP-MS at the State Key Laboratory of Geological Processes and Mineral Resources in China University of Geosciences, using a pulsed 193 nm ArF Excimer laser with $14 \text{ J} \cdot \text{cm}^{-2}$ energy density at a repetition rate of 8 Hz coupled to an Agilent 7500 quadrupole ICPMS with a spot size of 32 μm . External calibration was performed relative to multiple-reference materials (BCR-2G and BHVO-2G for garnet; GJ-1 and NIST 610 for zircon) combined with internal standardization (Si for garnet and zircon). Off-line selection and integration of background and analytical signals, time-drift correction and quantitative calibration were performed by ICPMSDataCal (Liu et al., 2008). The U.S. Geological Survey SRM BIR-1G glass standard was used to monitor external reproducibility and instrument drift. During the time-resolved analysis of minerals, contaminations resulting from inclusions, fractures, and zones of different composition were monitored using several elements, and only the relevant part of the signal was integrated. Analyses of rock standards (BCR-2G, BHVO-2G, GJ-1, NIST 610) indicate that the precision (RSD%) is better than 10% (2σ) for these elements.

Zircon U–Pb dating was done using the LA-ICPMS at the State Key Laboratory of Geological Processes and Mineral Resources, China University of Geosciences using the same parameters as with the zircon elemental analysis above. Zircon standard 91500 was used to normalize fractionation during analysis. Zircon standard GJ-1 was analyzed as a secondary standard for four times each sample. Time-dependent drifts of U–Th–Pb isotopic ratios were corrected using a linear interpolation for every fifth sample analysis according to the variations of the four 91500 analyses. The uncertainty of the preferred value for the external standard 91500 (0.9–1.3%, 1σ RSD) for $^{206}\text{Pb}/^{238}\text{U}$, was propagated into the ultimate results of the samples.

The U–Pb isotope compositions of those zircon grains with a narrow (less than 30 μm) metamorphic rim were obtained using a CAMECA IMS-1280 ion probe, at the Institute of Geology and Geophysics at the Chinese Academy of Sciences in Beijing. A focus O^- beam of $\sim 0.2 \text{ nA}$ intensity, resulting in pits with diameters of $\sim 20 \mu\text{m}$, was used in the analysis of these zircons (Li et al., 2009). Detailed analytical procedures followed Liu et al. (2011). Secondary ions were accelerated at 10 kV and analyzed at a mass resolution of ~ 5400 . The measured U–Th–Pb ratio and the elemental concentrations were corrected using reference zircon M257 (Nasdala et al., 2008). The measured compositions were corrected for common Pb using non-radiogenic ^{204}Pb (Stacey and Kramers, 1975).

The argon isotope ratios of hornblende were analyzed using a GVI-5400 noble gas mass spectrometer in the Guangzhou Institute of Geochemistry, Chinese Academy of Sciences, using the stepwise crushing technique (Qiu and Wijbrans, 2006). Samples and monitor standard DRA1 sanidine (Wijbrans et al., 1995) with an assumed age of $25.26 \pm 0.07 \text{ Ma}$ were irradiated at the 49–2 reactor in Beijing for 54 h. The crushing experiments were carried out in an in-house designed crushing apparatus which was connected to the extraction line. The extraction and purification lines were baked out for 20 h at $150 \text{ }^\circ\text{C}$ with heating tape, and the sample chamber was baked out with a furnace. The static blank of ^{40}Ar after 5 min was approximately 2 mV. The correction factors for interfering argon isotopes derived from Ca and K are as follows: $(^{39}\text{Ar}/^{37}\text{Ar})_{\text{Ca}} = 8.984 \times 10^{-4}$, $(^{36}\text{Ar}/^{37}\text{Ar})_{\text{Ca}} = 2.673 \times 10^{-4}$ and $(^{40}\text{Ar}/^{39}\text{Ar})_{\text{K}} = 5.97 \times 10^{-3}$. Experimental details can be found in Qiu and Wijbrans (2006).

The Lu–Hf and Sm–Nd isotope analyses were conducted on a ThermoElectron Neptune™ multi-collector (MC-) ICP-MS in the GeoAnalytical Laboratory at Washington State University. Sample dissolution and chemical separations are described by Cheng et al. (2008). Two different procedures were applied: (1) The minerals and one set of whole rock powders were digested using a selective tabletop procedure (Savillex-digested) which efficiently dissolves the target phase (e.g. garnet), but leaves behind microscopic refractory Hf-bearing phases such as zircon (Cheng et al., 2009). (2) One whole rock powder

split of each sample was digested by a second protocol which used high pressure Teflon bombs (Bomb-digested) to ensure total dissolution of refractory phases including zircon. Protocols for isotope analyses and data reductions are described by Vervoort et al. (2004). Hafnium and Nd isotopic compositions were corrected for mass fractionation with the exponential law using $^{179}\text{Hf}/^{177}\text{Hf} = 0.7325$ and $^{146}\text{Nd}/^{144}\text{Nd} = 0.7219$, and normalized relative to the JMC475 Hf ($^{176}\text{Hf}/^{177}\text{Hf} = 0.282160$) and WSU's in-house Ames Nd standards ($^{143}\text{Nd}/^{144}\text{Nd} = 0.512138$), respectively. Samarium isotope compositions were corrected for Gd and Nd interferences and $^{149}\text{Sm}/^{152}\text{Sm}$ ratios were fractionation-corrected using $^{147}\text{Sm}/^{152}\text{Sm} = 0.56081$. The overall external uncertainties of 0.5% and 0.0035% were applied to the measured $^{147}\text{Sm}/^{144}\text{Nd}$ and $^{143}\text{Nd}/^{144}\text{Nd}$, respectively, based on the long-term reproducibility of external rock standards. External uncertainties applied to measured data are 0.5% for $^{176}\text{Lu}/^{177}\text{Hf}$ and a combination of 2σ in-run error and a blanket 0.005% uncertainty added in quadrature for $^{176}\text{Hf}/^{177}\text{Hf}$. Epsilon Hf and Nd values were calculated using $^{176}\text{Hf}/^{177}\text{Hf} = 0.282785$, $^{176}\text{Lu}/^{177}\text{Hf} = 0.0336$, $^{143}\text{Nd}/^{144}\text{Nd} = 0.512630$ and $^{147}\text{Sm}/^{144}\text{Nd} = 0.1960$ for CHUR (Bouvier et al., 2008).

4. Geochemistry of bulk rock

Nine eclogite samples have similar major elemental composition and are of basaltic composition (Table 1). The rocks have high TiO_2 (3.05–3.83 wt%) contents. Their high $\text{K}_2\text{O} + \text{Na}_2\text{O}$ (3.39–4.04 wt%) and P_2O_5 (0.26–0.67 wt%) contents and relatively low MgO (4.84–6.01 wt%) suggest a slightly alkaline tholeiitic composition (Lebas, 1989). Chondrite-normalized rare earth element (REE) distribution patterns show a LREE-enriched pattern without Eu anomaly (Fig. 2a). The eclogites have similar MORB-normalized trace element patterns showing enrichment in Rb and Ba, marked negative Sr anomalies, and no significant depletion in Ta, Nb, Zr, and Hf (Fig. 2b).

5. Petrography and mineral compositions

The Bailang eclogite samples have mineral assemblages involving idiomorphic garnet ($\sim 45 \text{ vol. } \%$; mostly 0.3–0.8 mm across) set in a matrix of omphacite ($\sim 30 \text{ vol. } \%$; 0.2–0.5 mm across), amphibole (10–20 vol. %), epidote ($\sim 5 \text{ vol. } \%$), phengite ($\sim 5 \text{ vol. } \%$), and minor rutile, quartz, paragonite and chlorite (Fig. 3). Only a small amount of glaucophane is present in eclogite, which is mostly retrogressed to hornblende (Fig. 3). Lawsonite is observed only as inclusion in garnet (Fig. 3d–f). Neither relic coesite nor typical quartz pseudomorphs after coesite were found within the samples.

Compositions of representative minerals are listed in Supplementary Tables 1–5. Garnet and clinopyroxene analyses are recalculated to twelve and six oxygen with estimation of Fe^{3+} by charge balance. Phengite formulae have all Fe expressed as Fe^{2+} . Nomenclature of amphibole contents follow Leake et al. (1997). The Fe^{3+} content of amphiboles were calculated using the method described by Schumacher (1991). Epidote formulas were calculated assuming 25 oxygen atoms and all iron as Fe^{3+} .

Porphyroblastic garnet commonly shows a core crowded with inclusions and an outer rim with much fewer inclusions. All garnet grains contain similar inclusions of epidote, omphacite, rutile, quartz, glaucophane, lawsonite, chlorite and box-shaped epidote + paragonite \pm phengite aggregates, probably pseudomorph after lawsonite (Fig. 3). All garnets are almandine-rich, ranging from 61–67 mol.% (Fig. 4a), and exhibit chemical zoning characteristics typical of prograde garnet growth, showing increasing pyrope and grossular as well as decreasing almandine and spessartine contents from core to rim (Fig. 5c).

Clinopyroxene usually occurs as small subhedral–anhedral grains in the matrix or as inclusions in garnet and epidote porphyroblasts (Fig. 3b). The clinopyroxene is omphacite according to Morimoto (1988) and shows a limited compositional variation and unzoned with jadeite content ranging from 41–47 mol.% (Fig. 4b). There is no significant

Table 1
Chemical compositions of the Bailang eclogite.

Sample	eclogite body I				eclogite body II					
	BL-a	BL-c	BL-d	BL-e	BL-f	BL-g	BL-h	BL-i	BL-b	
<i>(Major oxides in wt.%)</i>										
SiO ₂	47.32	47.44	47.69	47.81	46.47	48.52	47.65	46.13	47.31	
TiO ₂	3.34	3.59	3.66	3.05	3.31	3.47	3.46	3.83	3.35	
Al ₂ O ₃	14.05	13.69	13.83	13.58	14.63	13.84	13.42	13.80	14.16	
Fe ₂ O ₃	3.65	3.80	3.8	3.32	3.28	4.31	3.40	3.69	4.18	
FeO	10.61	10.69	11.05	9.98	11.41	10.17	11.25	10.64	9.98	
MnO	0.22	0.22	0.21	0.19	0.24	0.22	0.23	0.21	0.23	
MgO	5.41	5.16	5.19	6.01	5.07	5.25	4.84	5.38	5.38	
CaO	9.07	8.76	8.93	10.6	8.44	8.12	8.90	9.25	8.31	
Na ₂ O	2.97	2.95	3.00	2.96	3.08	2.95	2.97	2.94	2.82	
K ₂ O	0.77	0.98	1.04	0.43	0.79	0.83	1.03	1.07	0.81	
P ₂ O ₅	0.44	0.56	0.67	0.26	0.46	0.40	0.62	0.67	0.39	
L.O.I.*	0.81	0.81	0.13	0.48	0.82	1.88	0.42	0.14	1.79	
H ₂ O	1.58	1.46	0.95	1.46	1.40	2.56	0.86	0.97	2.51	
CO ₂	0.32	0.47	0.27	0.13	0.52	0.37	0.76	0.27	0.36	
Total	100.47	100.00	100.42	100.26	99.63	100.61	99.49	99.89	101.58	
<i>(Trace elements in ppm)</i>										
La	25.8	26.9	28.8	18.0	30.0	25.0	25.8	29.9	26.3	
Ce	56.1	57.4	62.9	37.6	67.5	54.1	57.7	60.3	56.5	
Pr	7.79	8.55	9.03	5.34	8.87	8.22	8.00	9.45	7.92	
Nd	35.5	37.6	41.3	23.5	42.3	34.7	38.8	39.5	34.8	
Sm	8.15	9.11	10.20	5.16	9.24	7.90	8.77	10.67	8.02	
Eu	2.55	2.92	3.34	1.69	2.63	2.55	2.71	3.49	2.52	
Gd	8.09	8.89	10.10	5.45	8.74	8.10	8.67	9.90	8.07	
Tb	1.28	1.42	1.53	0.94	1.37	1.35	1.41	1.50	1.30	
Dy	6.87	7.53	7.95	5.20	7.20	7.27	7.46	7.84	7.13	
Ho	1.33	1.41	1.47	1.00	1.51	1.34	1.37	1.50	1.35	
Er	3.48	3.61	3.84	2.68	3.71	3.53	3.54	3.75	3.70	
Tm	0.52	0.53	0.55	0.39	0.58	0.54	0.47	0.57	0.54	
Yb	2.78	2.78	2.87	2.16	3.13	3.04	2.56	2.73	2.94	
Lu	0.41	0.41	0.40	0.33	0.46	0.47	0.37	0.40	0.45	
Y	33.4	36.3	38.0	25.7	35.2	33.5	35.9	39.7	34.7	
Sc	35.6	34.1	33.5	40.9	31.2	35.1	35.3	31.9	36.7	
Cr	38.8	39.7	33.2	47.2	26.4	49.2	36.8	33.3	48.3	
Rb	22.2	25.2	23.2	11.2	26.2	28.0	23.3	24.2	28.1	
Nb	24.5	25.2	21.9	20.5	23.9	30.4	22.2	23.0	31.8	
Cs	1.78	1.44	0.61	0.80	2.57	3.24	0.49	0.58	3.15	
Ta	1.38	1.43	1.44	1.10	1.43	1.56	1.33	1.40	1.56	
Pb	6.41	5.25	4.13	7.79	6.15	7.68	3.92	4.14	7.55	
Th	3.10	2.88	2.66	2.64	3.93	3.14	2.97	2.54	3.18	
Ni	40.7	38.9	37.8	55.0	29.5	41.2	37.9	37.5	40.6	
V	320	339	357	289	302	315	362	340	330	
Ba	359	415	529	248	322	336	371	540	337	
Sr	245	237	235	312	192	229	250	232	239	
Zr	216	212	204	152	279	219	215	202	227	
Hf	7.20	7.03	6.81	5.07	9.39	7.22	7.15	6.73	7.55	

composition difference between omphacite in the matrix and in inclusions.

Phengite commonly occurs as subhedral fine-grained flakes defining a weak foliation together with glaucophane and omphacite. Paragonite also occurs as a constituent together with epidote and/or phengite in box-shaped aggregates included in garnet, which are interpreted as pseudomorphs after lawsonite (Fig. 3). Phengite is dominated by Mg-celadonite substitution and has Si contents of 3.57–3.64 and Mg + Fe²⁺ values of 0.59–0.73 atoms per formula units (*a.p.f.u.*) on the basis of eleven oxygen. Phengite inclusions in garnet show lower Si contents of Si = 3.31–3.36 than that in the matrix (Fig. 4c). Amphibole is grouped into glaucophane and hornblende amphibole after Leake et al. (1997; Fig. 4d). Glaucophane appears as small grains or as inclusions in garnet, few large glaucophane porphyroblasts are also observed to overgrow the matrix (Fig. 3b). Hornblende amphiboles appear as rims of glaucophane or as fine grains in the matrix and are mostly Mg-hornblende (Fig. 4).

Lawsonite is rare and only preserved as small inclusions in garnet (Fig. 3d–f). It is worth noting that lawsonite inclusions occur both in garnet core and rim. Larger lawsonite inclusions in garnet are generally

replaced by fine-grained aggregates of epidote and paragonite (Fig. 3e). Lawsonite has not been observed in the matrix, either as preserved crystals or as its pseudomorphic replacements. Lawsonites have ~1.0 Ca *a.p.f.u.* and low Fe/(Fe + Al) ratios (≤ 0.02). Epidote commonly occurs as inclusions in garnet and as porphyroblasts in the matrix and with inclusions of garnet, glaucophane and rutile. The epidotes show limited compositional range with $X_{Fe^{3+}} = (Fe^{3+}/[Fe^{3+} + Al]) = 0.16–0.19$ and Ca = 1.98–2.01 *a.p.f.u.* Rare chlorite is present as inclusions in garnet and as a matrix phase with Mg# ranging from ~50 (inclusion in garnet) to ~57 (matrix). Very rare talc was identified as inclusion in garnet.

6. Geochronology

6.1. U–Pb chronometer and REE data

The zircon crystals in the eclogites are transparent and colorless. They occur as anhedral to euhedral crystals (40–200 μm in diameter), with length/width ratios of 1:1–2.5:1. They show a core with unzoned or sector-zoned CL responses (Fig. 6a), surrounded by an overgrowth rim (mostly less than 30 μm in width) with weak CL (Fig. 7a). Inclusions

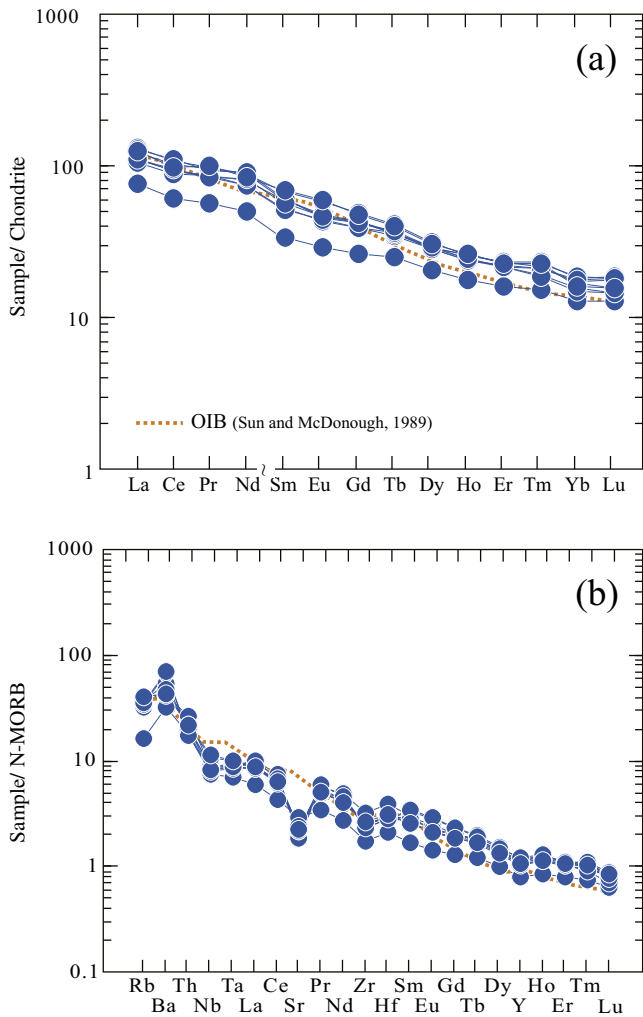


Fig. 2. Chondrite-normalized REE patterns (a) and N-MORB normalized trace-element patterns (b) for the Bailang eclogite. The compositions of chondrite and oceanic island basalt (OIB) are after Sun and McDonough (1989).

of garnet, omphacite and phengite were identified in the zircon rim (Fig. 7b). Due to the narrow width of the zircon rim, we used SIMS to date these zircon rims and LA-ICPMS for the cores.

The zircon cores have high U (216–10722 ppm) and high Th/U ratios (0.24–2.33), and show HREEs enrichment and negative Eu anomalies in normalized REE patterns (Fig. 6b). Thirty five analyses on 28 zircon grains are reported in Table 2 and presented in Fig. 6a. Analyses yield scattered concordant and discordant U–Pb ages, with an older population of concordant cores ages from about 1.0 to 0.6 Ga and a somewhat narrower but still broad range of ages from 320 to 270 Ma. We calculated a weighted mean $^{206}\text{Pb}/^{238}\text{U}$ age of 304 ± 5 Ma (MSWD = 5) for twenty-two concordant analyses from the younger population. The age probability distribution diagram (inset of Fig. 6a) shows peaks at ~283 Ma and ~306 Ma.

The zircon rims have very low U contents of 1.1–4.7 ppm, resulting in low amounts of radiogenic Pb and, therefore, high analytical uncertainties. In the chondrite-normalized pattern (Fig. 7c), the rims have rather flat HREE patterns and an absence of a negative Eu anomaly. All analyses exhibit low LREE abundances, with some containing La and Pr at or below detection levels (Table 3). Eighteen analyses scatter in apparent age between 215 and 245 Ma, defining a lower intercept age of 227.4 ± 6.4 Ma (MSWD = 1.8).

6.2. Lu–Hf and Sm–Nd isotopic data

We analyzed handpicked separates of garnet and the corresponding whole rock and/or omphacite and summarized the isotopic results in Table 4 and Fig. 8. The parent/daughter ratios of Lu/Hf and Sm/Nd for garnets are 4.2–7.1 and 1.1–1.2, suggesting that garnet fractionates Lu from Hf more strongly than Sm from Nd, which is consistent with experimental partition coefficients (Green et al., 2000). The six garnet fractions from the Bailang eclogite have Nd concentrations of ~1.1 ppm and $^{147}\text{Sm}/^{144}\text{Nd}$ ratios of ~0.7 (Table 4), comparable to the Nd contents (0.4–1.8 ppm) and the Sm/Nd ratios (0.9–3.0) across single garnet. Garnet fractions have rather low Hf contents of ~0.1 ppm, producing less precise Hf isotope analyses than the whole rock. The bomb-digested whole rocks have much higher Hf concentrations than those of the Savillex-digested splits.

Lu–Hf and Sm–Nd ages were calculated using the ^{176}Lu decay constant of 1.867×10^{-11} (Scherer et al., 2001; Söderlund et al., 2004) and the ^{147}Sm decay constant of 6.54×10^{-12} (Lugmair and Marti, 1977), respectively. Errors are reported at 95% confidence. Isochrons were constrained by Savillex-digested whole rock, bomb-digested whole rock, garnet, and/or omphacite aliquots. We did not analyze Lu–Hf isotope for omphacites due to their extremely low Lu (≤ 1 ppb) and Hf (≤ 60 ppb) concentrations, which would produce rather low precision isotope results. The six garnet fractions combined with two whole rocks yield a Lu–Hf age of 238.1 ± 3.6 Ma (2σ , MSWD = 5.4) and a corresponding Sm–Nd age of 230.0 ± 4.7 Ma (2σ , MSWD = 0.3). The initial isotope values calculated for these isochrons are $^{176}\text{Hf}/^{177}\text{Hf} = 0.28296 \pm 3$ and $^{143}\text{Nd}/^{144}\text{Nd} = 0.51267 \pm 2$, corresponding to initial epsilon values calculated at their metamorphic ages of $\epsilon_{\text{Hf}(t=240 \text{ Ma})} = +11.5$ and $\epsilon_{\text{Nd}(t=230 \text{ Ma})} = +6.5$. Including the bomb-digested whole rocks improves the precision of the Lu–Hf regression and yields similar initial isotopic values.

6.3. Ar isotopic data

The multi-grain laser step-heating $^{40}\text{Ar}/^{39}\text{Ar}$ dating results of the amphibole are shown in supplemental materials, and the age spectrum and isochron plot are shown in Fig. 9. The $^{40}\text{Ar}/^{39}\text{Ar}$ dating results are calculated using the ArArCALC program (Koppers, 2002). The Ar release pattern of hornblende is slightly scattered, allowing calculation of a total fusion age of 198.7 ± 2.6 Ma. Excluding the first and the last increments of the Ar-release spectrum with large errors, a poorly weighted plateau age of 200.5 ± 7.2 Ma from steps 2–10 is defined. The inverse isochron diagram of $^{36}\text{Ar}/^{40}\text{Ar}$ vs $^{39}\text{Ar}/^{40}\text{Ar}$ yields a similar age of 207 ± 15 Ma and has an initial $^{40}\text{Ar}/^{36}\text{Ar}$ ratio of 282 ± 34 , comparable to the present day atmospheric composition of Ar.

7. Discussion

7.1. The metamorphic P–T evolution of the Bailang eclogite

Garnet compositional profiles and the change of the inclusion mineralogy within garnet recorded the prograde P–T conditions of the Bailang eclogite. The typical zoning pattern of garnet, with cores enriched in Mn and Ca and rims enriched in Mg, appears to suggest prograde growth zoning at low P–T conditions. The observed inclusion mineralogy in garnet is largely identical and includes epidote, glaucophane, lawsonite, chlorite and quartz. Therefore, garnet appears to have grown within the lawsonite stability condition and passed chlorite stability at lower P–T condition, probably at blueschist-facies stage. The increasing Mg content towards garnet rim, together with the occurrence of omphacite and phengite inclusions, suggest garnet rim grew at an elevated P–T condition. When present, chlorite inclusions in garnet rims are always on the cracks connected with the matrix, and the presence of chlorite replacing garnet at its rims (Fig. 3) suggests those chlorites are a later phase. This, together with the hornblende amphibole

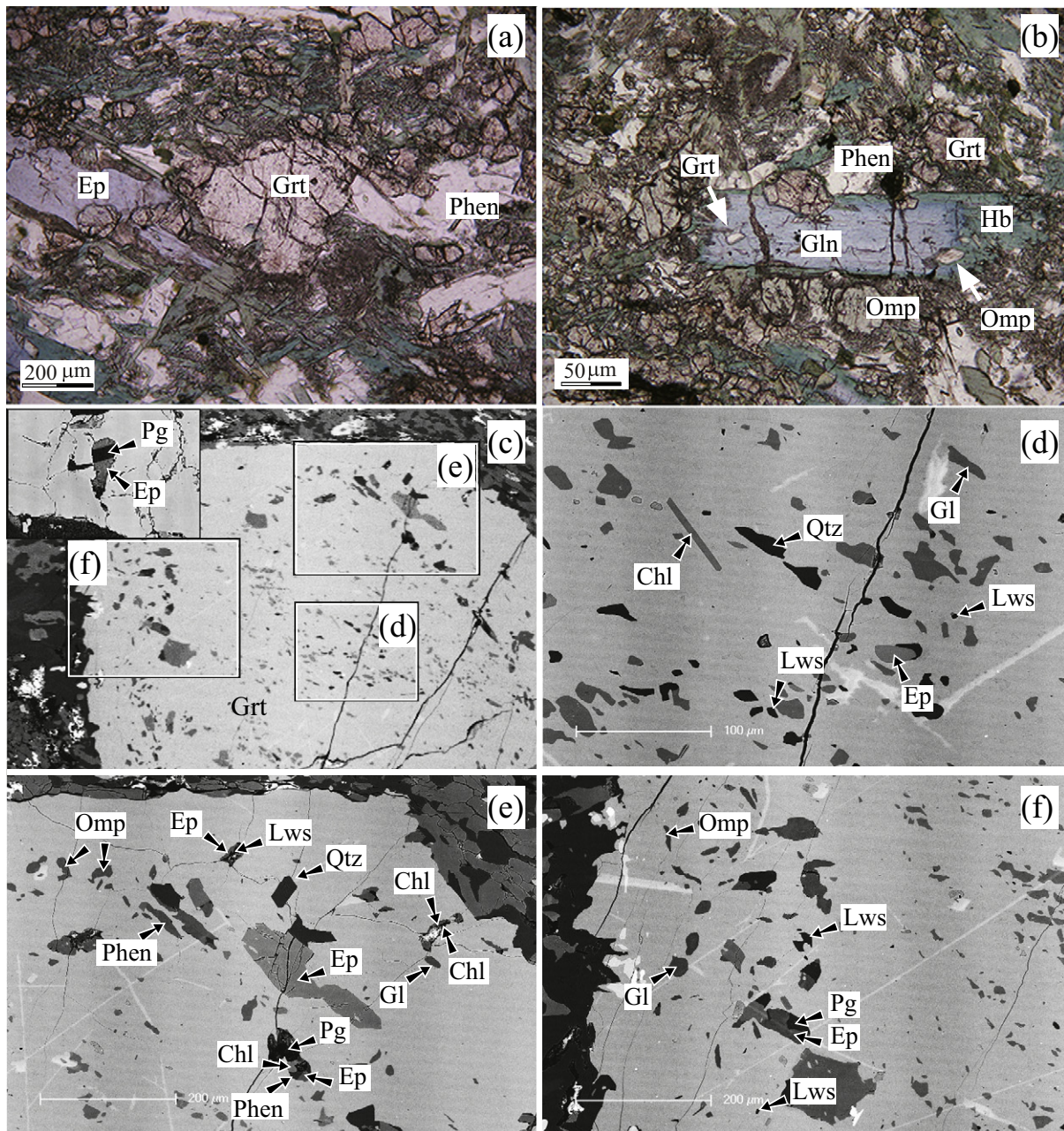


Fig. 3. Photomicrographs and backscattered-electron images of the Bailang eclogite. Mineral abbreviations used are: Chl, chlorite; Ep, epidote; Gl, glaucophane; Grt, garnet; Hb, hornblende amphibole; Lws, lawsonite; Phen, phengitic muscovite; Omp, omphacite; Pg, paragonite; Q, quartz. (Note lawsonite inclusions, and the epidote-paragonite pseudomorphs after lawsonite in garnet).

rim of glaucophane and the presence of box-shaped epidote + paragonite ± phengite ± chlorite aggregates, which are interpreted as pseudomorphs after lawsonite, indicate a post eclogite-stage through epidote-amphibolite-facies to greenschist-facies overprinting.

The peak metamorphic conditions of the Bailang eclogite are estimated by a combined Fe^{2+} -Mg exchange thermometer (Krogh-Ravna, 2000) and garnet-clinopyroxene-phengite- SiO_2 barometric calibration (Krogh-Ravna and Terry, 2004) coded in an Excel spreadsheet (Krogh-Ravna and Terry, 2004). Garnet rim analyses with a maximum pyrope and the Si-richest phengite analysis were used to estimate the peak pressure and temperature for the eclogite-facies metamorphism. Where the rim compositions of garnet-omphacite pairs were found in textural equilibrium, the estimated maximum pressure and temperature intervals were within the range of 2.5–2.7 GPa and 465–503 °C.

To further constrain the metamorphic evolution, and to complement P - T estimates from the traditional thermobarometry for the Bailang eclogite, P - T pseudosections were calculated for the P - T range of 1.6–2.8 GPa and 400–600 °C (Fig. 10a) in the NCKMnFMASHO system (Na_2O - CaO - K_2O - MnO - FeO - MgO - Al_2O_3 - SiO_2 - H_2O - O) considering the mineral assemblages and compositions discussed above, and the internally consistent thermodynamic dataset of Holland and Powell (1998, updated 2002). Quartz/coesite was considered to be in excess. It is notable that the quartz/coesite transition line would shift towards lower pressure if using the thermodynamic dataset of Berman (1988). The fluid phase was assumed to be pure H_2O and was considered to be in excess. Because garnet is chemically zoned in studied sample, the bulk-rock compositions may have been fractionated during garnet growth (e.g., Evans, 2004). Therefore it is critical to generate an effective bulk

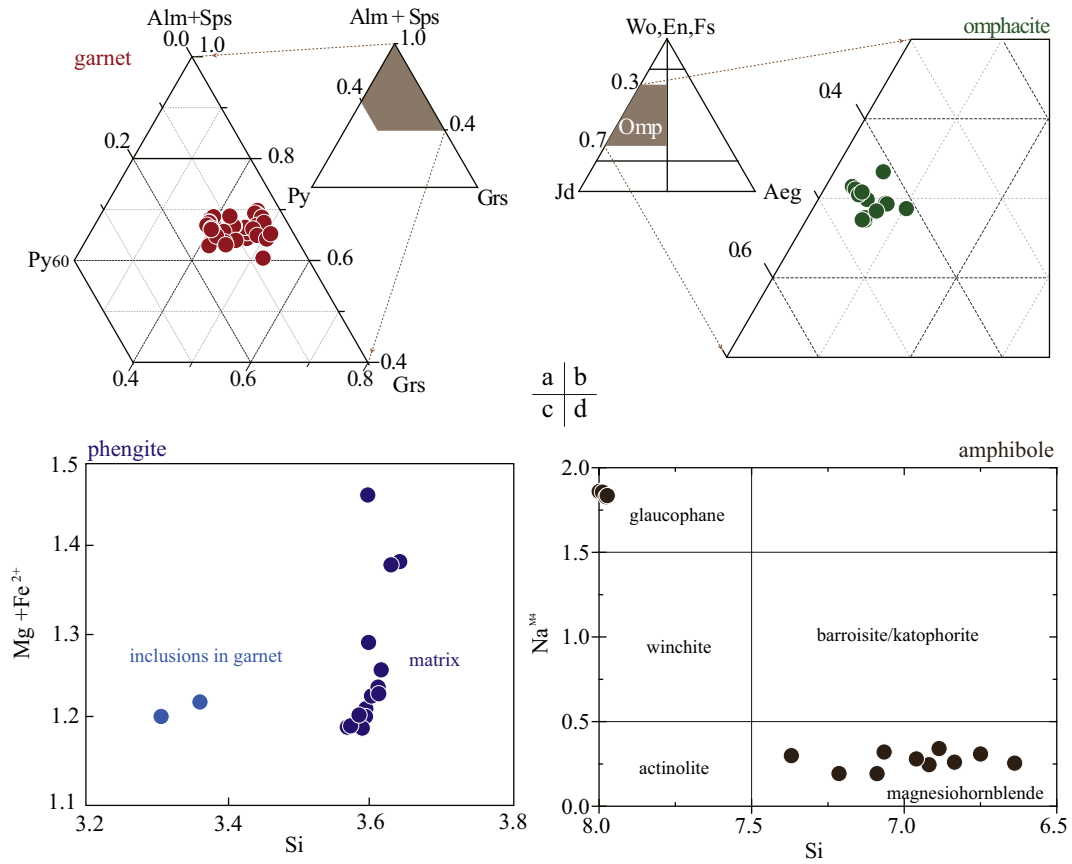


Fig. 4. Compositional diagrams showing range of (a) garnet, (b) omphacite, (c) phengite, and (d) amphibole.

composition for phase equilibrium calculations in garnet-bearing rocks. For the studied eclogite, the effective bulk composition (Fig. 10) was calculated following the method described by Evans (2004) based on a Rayleigh fractionation model of the measured Mn content of garnet, obtained by subtracting garnet core from the XRF-based bulk composition (Table 1; supplemental materials), was normalized in the NCKMnFMASHO system. The Fe³⁺ amount value is estimated based on the mode and composition of the major Fe-bearing minerals determined with the electron probe and calculated to structural formulae considering Fe²⁺+Fe³⁺ in supplemental materials.

Pseudosections were calculated using the software PERPLE_X (version 6.6.9; Connolly, 2005). The CORK model (Holland and Powell, 1998) was used for the equation of state of fluid. Solid-solution models used are: garnet (White et al., 2007), clinopyroxene and amphibole (Diener and Powell, 2012), chlorite (White et al., 2014), epidote and talc (Holland and Powell, 1998) and white mica (Smye et al., 2010). Lawsonite, quartz, kyanite, talc and rutile were considered to be pure phases. The final pseudosections and contoured P–T diagram were redrawn by smoothing curves as demonstrated by Connolly (2005) and shown in Fig. 10a. The garnet core–rim zoning (A → B in Fig. 5) is modelled to yield a P–T path from ~1.8 GPa at ~454 °C in the g + o + chl + mu + law + q field to ~2.5 GPa at ~491 °C in the g + o + gl + mu + law + q field. The maximum Si = 3.65 *a.p.f.u.* in phengite is estimated to reflect a pressure of ~2.5 GPa at ~490 °C, in agreement with the P–T condition defined by garnet rim compositions. Interestingly, our resultant diagram apparently is topologically very similar to the "Type-a" Tianshan eclogite (Tian and Wei, 2014), showing an unexpected large P–T stability field of chlorite. Pseudosection modelling constrained peak P–T conditions resembling those determined by conventional thermobarometry. The agreement between conventional thermobarometry and pseudosection modelling methods supports the choice of equilibrium mineral compositions and

suggests that the estimated P–T conditions of peak metamorphism are robust within their uncertainties.

The calculated peak P–T conditions for the Bailang eclogite are considerably lower than previous estimate of 650–790 °C and 3.3–3.9 GPa for other eclogites in this area (Li et al., 2007; Yang et al., 2009; Zhang et al., 2011; Cheng et al., 2012). The Sumdo, Jilang and Bailang eclogites come from a small portion of the Lhasa terrane, spanning ~10 km north to south and ~30 km west to east (Fig. 1b). Does such a diversion of peak metamorphic conditions (Fig. 10b) mean that this entire area was subjected to (U)HP metamorphism as a single block, or is it possible that this region comprises different slices that had distinct P–T histories and hence underwent (U)HP metamorphism at different times?

7.2. Age interpretation

7.2.1. Zircon U–Pb

Zircon in HP/UHP metamorphic rocks can preserve inheritance and crystallize at different metamorphic episodes during subduction and exhumation due to its temperature resistance and chemical robustness. The zircon cores from the eclogite are characterized by igneous growth zoning, or no zoning, a stronger CL intensity, high Th/U ratios and high U concentrations, a clear negative Eu anomaly and a positive Ce anomaly, as well as HREE enriched patterns (Fig. 6a). These textural and chemical features suggest that the cores are magmatic zircon crystals inherited from the protoliths (Hoskin and Black, 2000; Corfu et al., 2003). The steep HREE patterns and pronounced negative Eu anomalies (Fig. 6b) imply that zircon growth is not in communication with garnet and/or zircon formed in an 'open' system, preventing any change in zircon composition due to the crystallization of garnet or other minerals. The high U contents, which are typical in the pegmatite, indicate that the zircon crystallized from a highly evolved hydrous melt system (Hoskin,

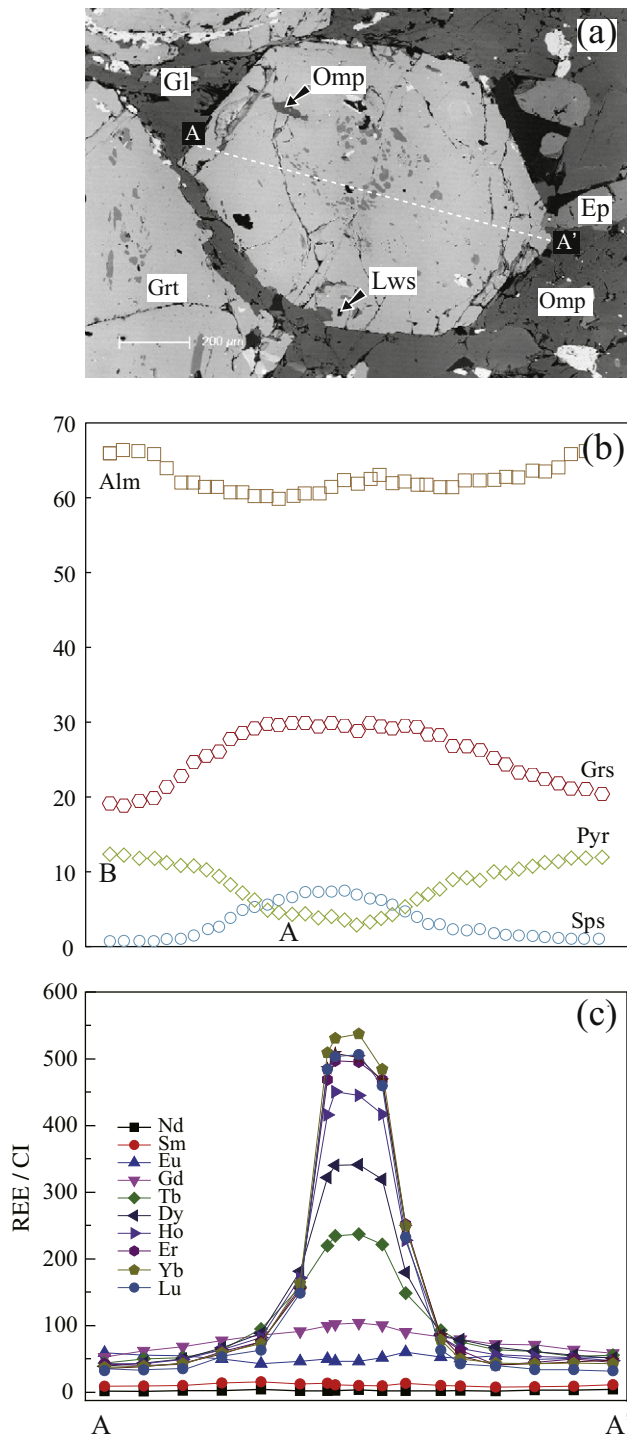


Fig. 5. Chemical profile through representative garnet grain from the Bailang eclogite.

2005; Rayner et al., 2005). The weighted mean $^{206}\text{Pb}/^{238}\text{U}$ age of 304 ± 5 Ma (2σ , MSWD=5) is considered an approximate estimate of the protolith formation age. The broad range in ages (inset of Fig. 6a) appears to suggest that the growth of zircon extends a period of several tens of million years (~306 to ~283 Ma).

The zircon rims are unzoned or weakly zoned and are thought to represent metamorphic overgrowths (Corfu et al., 2003; Hanchar and Hoskin, 2003). The age of the overgrowth rims is not well constrained due to the low U contents and the limited width, with apparent $^{206}\text{Pb}/^{238}\text{U}$ ages scattering between 215 and 245 Ma (Fig. 7a). Garnet, omphacite and phengite inclusions (Fig. 7b) were found within this

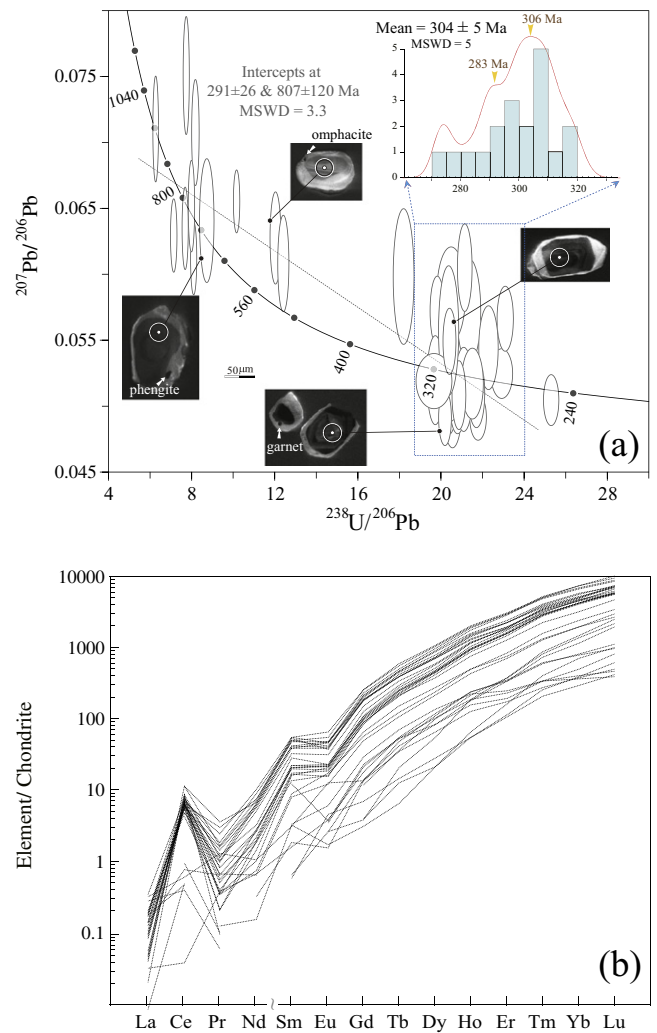


Fig. 6. (a) Tera-Wasserburg plot for uncorrected LA-ICPMS U-Pb analysis for zircon cores from the Bailang eclogite. Ages are intercept ages forced to the model common Pb composition of Stacey and Kramers (1975). Representative CL images of zircon are also shown. (b) REE patterns of dated zircon crystals.

domain, providing evidence that the overgrowth formed during eclogite-facies metamorphism. The REE pattern of these rims of zircon was characterized by flat HREEs and no significant Eu anomaly (Fig. 7c), again suggesting growth beyond the stability of feldspar at high pressure in the presence of garnet (Rubatto, 2002). The progressive HREE depletion in the overgrowths is interpreted as the consequence of concomitant garnet crystallization. Therefore, 243 ± 6 Ma is taken as the maximum estimate for the timing of eclogite-facies metamorphism.

7.2.2. Garnet Lu-Hf and Sm-Nd

Due to the small size of the garnet grain, which would not yield enough amount of Lu/Hf and Sm/Nd for isotope analysis (Cheng et al., 2008), multi-grain garnet fractions were picked for Lu-Hf and Sm-Nd isotope analysis. No attempt has been made to separate different garnet growth zones or generations. Because garnet crystals may grow slowly over a prolonged time span, the bulk garnet ages could represent any timing within the overall garnet growth interval, i.e., how accurately the analyzed garnet separates reflect the complete garnet chemistry within the rock. Furthermore, to clarify the geological meanings of these ages, inherited Hf-Nd, complexities in garnet growth and post-garnet crystallization resetting must be clarified carefully. Garnet grains from the Bailang eclogite were dated using both the ^{176}Lu - ^{176}Hf and ^{147}Sm - ^{143}Nd decay systems. Using the same grain separates for both

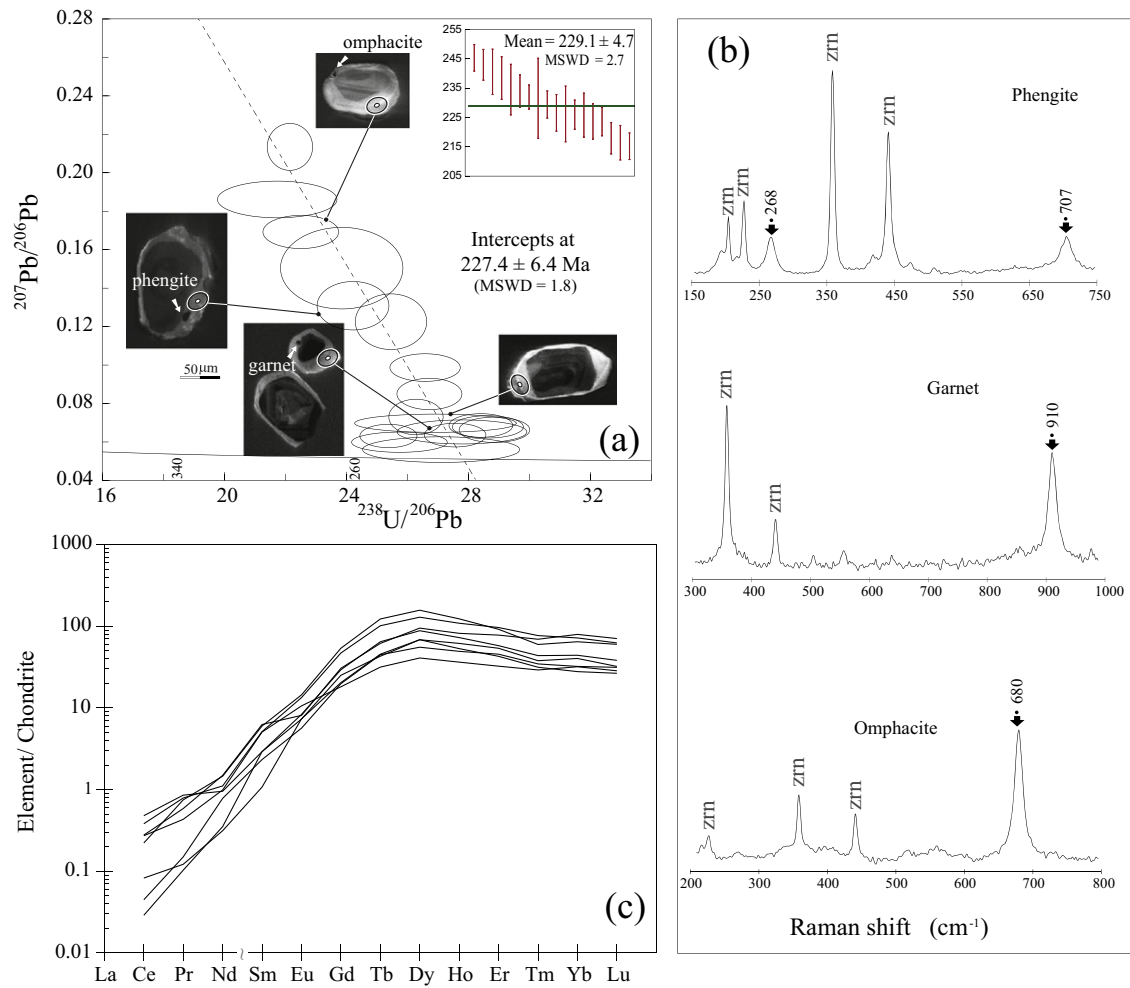


Fig. 7. (a) Tera-Wasserburg plot for uncorrected SIMS U–Pb analysis for zircon rims from the Bailang eclogite. Ages are intercept ages forced to the model common Pb composition of [Stacey and Kramers \(1975\)](#). Representative CL images of zircon are also shown. (b) Representative Raman spectra of garnet, omphacite and phengite inclusions in zircon. (c) REE patterns of dated zircon crystals.

isotope systems, we determined a Lu–Hf isochron age of 238.1 ± 3.6 Ma (2σ , $\text{MSWD} = 5.4$) and a slightly younger Sm–Nd isochron age of 230.0 ± 4.7 Ma (2σ , $\text{MSWD} = 0.3$).

The ca. 230 Ma Sm–Nd age is interpreted to reflect the formation of garnet rims and record the timing of eclogite-facies metamorphism for the following reasons: (1) the metamorphic temperature did not exceed the Sm–Nd closure temperatures, and there was no significant post-growth diffusive re-equilibration in the garnets; (2) the occurrence of the omphacite inclusions in garnet rims ([Fig. 3e,f](#)), indicating that the garnet rim growth occurred during eclogite-facies metamorphism; and (3) the cleaner garnet rim was preferentially selected during sample preparation and this garnet shell will strongly bias the age towards the rim formation due to the spherical geometry effect (the outer shells dominate the volume and thus control the Sm budget for the digested bulk garnet fractions; [Cheng et al., 2009](#)), which is enhanced by the slightly increasing Sm from core to rim of garnet ([Fig. 5c](#)). In contrast, the ca. 238 Ma Lu–Hf age is interpreted to the formation time of garnet core and pre-date the timing of eclogite-facies metamorphism due to the strongly Rayleigh-like zoned Lu in garnet, which would biased the bulk Lu to that of core as evidenced by the higher Lu content (~ 1.0 ppm) obtained by isotopic digestion than those of the garnet rim (~ 0.6 ppm).

The difference between Lu–Hf and Sm–Nd ages defines an 8.1 ± 5.9 Myr time span. There are several potential interpretations for the difference in age between the Lu–Hf and Sm–Nd systems: (a) the age difference is attributed to a higher closure temperature for Lu–Hf as

compared to Sm–Nd ([Scherer et al., 2000](#)); (b) Lu partitions strongly into garnet during growth yielding ages skewed towards the beginning of growth, while no similar partitioning for Sm–Nd and the age reflect mean garnet growth ([Lapen et al., 2003](#)); (c) Lu diffuses much faster than the highly charged Hf^{4+} resulting in Lu transfer from high Lu regions after formation, leading to anomalously old age ([Bloch et al., 2010](#); [Ganguly et al., 2011](#)); (d) the Sm–Nd system has been altered due to migration of Sm into or out of the garnet grain subsequent to garnet growth due to successive resorption ([Kelly et al., 2011](#)) or a diffusion limited REE uptake process ([Skora et al., 2006](#)); (e) the Lu–Hf system has been contaminated by inherited Hf-rich inclusions such as zircon and rutile, and/or the Sm–Nd system was contaminated by LREE-rich inclusions such as apatite and monazite ([Scherer et al., 2000](#)).

Closure temperature estimates (T_c ; [Dodson, 1973](#)) of the Sm–Nd system are function of grain size, thermal history and elemental zoning in garnet, all of which can vary widely, and could range from 480 to 900 °C (e.g., [Mezger et al., 1992](#); [Ganguly et al., 1998](#); [Scherer et al., 2000](#)) but is generally considered to be in the range of ~ 700 °C for garnet grains > 1 mm ([Smit et al., 2013](#)). The Lu–Hf system, in comparison, appears to close at a temperature higher than that of the Sm–Nd system ([Scherer et al., 2000](#); [Smit et al., 2013](#)) at the same conditions. The garnet and omphacite in the Bailang eclogite appear to have formed during eclogite conditions at a temperature below 481 °C, which is below the closure temperatures for the Lu–Hf and Sm–Nd systems in garnet. Experimental results indicate that Sm/Nd diffusion rates are slower ([Van Orman et al., 2002](#); [Carlson, 2012](#)) than those of major elements,

Table 2
LA-ICPMS U–Pb isotopic data for magmatic zircon cores from the Bailang eclogite.

spot	Element (ppm)			Isotopic ratios				Age (Ma)							
	U	Th	Th/U	²⁰⁷ Pb/ ²⁰⁶ Pb	1σ (%)	²⁰⁷ Pb/ ²³⁵ U	1σ (%)	²⁰⁶ Pb/ ²³⁸ U	1σ (%)	²⁰⁷ Pb/ ²⁰⁶ Pb	1σ	²⁰⁷ Pb/ ²³⁵ U	1σ	²⁰⁶ Pb/ ²³⁸ U	1σ
#1	448	384	0.86	0.07163	4.4	1.19217	4.0	0.12220	1.5	976	89	797	22	743	10
#2	10722	12289	1.15	0.05176	2.3	0.31561	2.8	0.04362	1.5	276	54	279	7	275	4
#3	3512	4334	1.23	0.05628	3.8	0.36950	4.9	0.04685	1.8	465	85	319	14	295	5
#4	1084	2027	1.87	0.05018	4.3	0.33377	4.1	0.04865	1.4	211	##	292	10	306	4
#5	1600	2378	1.49	0.05789	3.9	0.39360	4.6	0.04881	2.2	524	85	337	13	307	7
#6	3383	5835	1.72	0.05598	3.0	0.33815	3.1	0.04331	1.1	450	67	296	8	273	3
#7	323	156	0.48	0.07100	4.6	1.27094	4.6	0.12974	1.6	967	94	833	26	786	12
#8	1565	2296	1.47	0.05672	3.2	0.39805	3.3	0.05046	1.1	480	70	340	9	317	4
#9	1197	2272	1.90	0.05115	4.3	0.34550	4.4	0.04909	1.4	256	98	301	11	309	4
#10	2994	5964	1.99	0.04979	3.2	0.33194	3.1	0.04808	1.2	187	74	291	8	303	3
#11	677	339	0.50	0.06233	3.9	0.71888	3.9	0.08308	1.4	687	77	550	17	514	7
#12	2985	5339	1.79	0.05983	3.7	0.39457	3.8	0.04729	1.1	598	80	338	11	298	3
#13	652	254	0.39	0.06074	4.3	0.67553	4.2	0.08055	1.4	632	60	524	17	499	7
#14	449	109	0.24	0.07093	4.0	1.56149	4.0	0.15946	1.4	955	81	955	25	954	13
#15	749	1058	1.41	0.06012	5.7	0.45325	6.0	0.05494	1.8	609	##	380	19	345	6
#16	2148	3234	1.51	0.05084	3.0	0.34246	2.8	0.04879	1.0	235	70	299	7	307	3
#17	1100	1327	1.21	0.05529	4.3	0.33677	4.1	0.04487	1.4	433	96	295	10	283	4
#18	4270	8110	1.90	0.04857	2.4	0.31110	2.6	0.04590	1.2	128	53	275	6	289	3
#19	1691	1281	0.76	0.06211	3.0	1.21547	3.3	0.14006	1.4	680	63	808	18	845	11
#20	831	677	0.81	0.06055	3.2	1.04198	3.2	0.12347	1.2	633	73	725	17	751	9
#21	867	954	1.10	0.05263	4.9	0.36325	4.5	0.05069	1.3	322	##	315	12	319	4
#22	1220	2254	1.85	0.05062	3.6	0.32394	3.6	0.04607	1.2	233	53	285	9	290	3
#23	982	1504	1.53	0.05112	4.3	0.33514	4.3	0.04741	1.4	256	##	293	11	299	4
#24	397	381	0.96	0.07436	4.0	1.33721	4.1	0.12918	1.3	1051	80	862	24	783	9
#25	457	529	1.16	0.06353	3.6	1.13834	3.5	0.13004	1.3	728	75	772	19	788	9
#26	1174	1171	1.00	0.05224	4.0	0.33147	3.8	0.04649	1.6	295	86	291	10	293	5
#27	216	175	0.81	0.06662	5.6	1.01189	5.5	0.11454	2.6	828	##	710	28	699	17
#28	2056	2657	1.29	0.04890	3.0	0.33533	3.0	0.04952	1.0	143	68	294	8	312	3
#29	1780	2269	1.27	0.05081	3.6	0.33596	3.5	0.04793	1.1	232	88	294	9	302	3
#30	655	889	1.36	0.05634	6.0	0.37727	6.0	0.04909	1.6	465	##	325	17	309	5
#31	524	328	0.63	0.06504	3.8	1.12429	3.7	0.12512	1.3	776	80	765	20	760	9
#32	1145	1272	1.11	0.05302	4.1	0.36393	3.9	0.05086	2.9	328	93	315	11	320	9
#33	4956	11529	2.33	0.05012	2.7	0.27496	2.7	0.03952	1.0	211	31	247	6	250	2
#34	1805	554	0.31	0.06507	2.6	0.88891	2.6	0.09838	1.0	776	56	646	12	605	6
#35	2180	3459	1.59	0.05426	3.1	0.37101	3.2	0.04900	1.0	389	70	320	9	308	3

depending on the composition of the garnet. The analyzed garnet grains in this study preserve bell-shaped spessartine profiles indicating prograde chemical zoning as a result of fractionation of Mn from the rock (Hollister, 1966). Thus, it is likely that the Sm–Nd systematics are also preserved from original growth. In this regard, the age difference cannot be solely attributed to a higher closure temperature for Lu–Hf as compared to Sm–Nd.

Table 3
SIMS U–Pb isotopic data for metamorphic zircon rims from the Bailang eclogite.

Spot	U	Th	²⁰⁶ Pb/ ²⁰⁴ Pb ^a		1σ (%)	²⁰⁷ Pb/ ²⁰⁶ Pb ^b		1σ (%)	²⁰⁶ Pb/ ²³⁸ U ^c	age (Ma) ^c
			238U/ ²⁰⁶ Pb	238U/ ²⁰⁶ Pb		207Pb/ ²⁰⁶ Pb	207Pb/ ²⁰⁶ Pb			
#1	2.0	b.d	95.7	25.3943	2.4	0.06	6.4	245.4 ± 4.5		
#2	1.9	0.1	172	21.7427	6.0	0.19	3.4	240.6 ± 7.7		
#3	1.7	b.d	83.8	25.7547	4.0	0.06	5.9	243.0 ± 5.3		
#6	1.9	0.2	8.47	23.8595	5.6	0.15	9.3	231.5 ± 13.7		
#7	47.0	b.d	52.5	27.5832	2.4	0.06	6.5	226.0 ± 5.0		
#8	11.1	b.d	63.8	27.8104	5.1	0.06	6.4	223.7 ± 6.1		
#9	2.5	b.d	7.80	26.5971	2.9	0.10	4.8	223.6 ± 4.9		
#10	3.6	b.d	213	25.4776	3.0	0.12	7.8	225.8 ± 7.5		
#11	2.5	b.d	83.8	24.2306	3.2	0.13	6.4	234.5 ± 8.6		
#12	3.2	b.d	23.4	28.6572	2.7	0.07	5.7	216.4 ± 5.9		
#13	2.8	b.d	54.2	28.8741	2.7	0.07	6.6	215.2 ± 4.5		
#14	2.0	b.d	40.1	22.5163	3.6	0.17	3.4	238.5 ± 7.3		
#15	2.6	b.d	63.8	22.1582	2.2	0.21	3.8	226.2 ± 9.5		
#18	3.1	b.d	43.7	26.2983	2.2	0.07	8.4	234.0 ± 5.6		
#20	3.0	b.d	54.2	27.1257	6.3	0.06	7.9	232.0 ± 4.1		
#22	4.2	b.d	40.1	26.9422	6.5	0.07	4.5	229.4 ± 4.6		
#23	2.1	b.d	8.47	26.7391	2.6	0.08	6.4	226.6 ± 6.3		
#24	2.6	b.d	7.80	28.4280	2.4	0.07	5.9	217.9 ± 5.4		

^a Measured value.

^b Uncorrected.

^c Ages are based on ²⁰⁷Pb corrected data; uncertainties are reported at the 1σ level.

Decoupling of Sm–Nd and Lu–Hf ages could potentially be utilized to retrieve cooling history of metamorphic rocks due to the different temperatures of diffusion-controlled isotopic closure for these two

Table 4
Lu–Hf and Sm–Nd isotope data for the Bailang eclogite.

Samples ^a	Lu (ppm)	Hf (ppm)	¹⁷⁶ Lu/ ¹⁷⁷ Hf ± 2σ		¹⁷⁶ Hf/ ¹⁷⁷ Hf [†] ± 2σ	
Grt.1	0.996	0.148	0.959	0.0048	0.287226	0.000009
Grt.2	0.982	0.171	0.813	0.0041	0.286554	0.000004
Grt.3	0.983	0.148	0.945	0.0047	0.287165	0.000010
Grt.5	0.983	0.139	1.005	0.0050	0.287495	0.000008
Grt.6	0.983	0.233	0.599	0.0030	0.285587	0.000007
WR.Bomb	0.467	6.96	0.00953	0.000048	0.283015	0.000004
WR.Sav	0.456	1.26	0.0515	0.00026	0.283169	0.000007
Samples	Sm (ppm)	Nd (ppm)	¹⁴⁷ Sm/ ¹⁴⁴ Nd ± 2σ		¹⁴³ Nd/ ¹⁴⁴ Nd [†] ± 2σ	
Grt.1	1.25	1.03	0.7302	0.0037	0.513774	0.000011
Grt.2	1.27	1.09	0.7062	0.0035	0.513734	0.000015
Grt.3	1.27	1.07	0.7171	0.0036	0.513754	0.000007
Grt.4	1.28	1.11	0.6979	0.0035	0.513726	0.000007
Grt.5	1.28	1.11	0.6974	0.0035	0.513720	0.000009
Grt.6	1.27	1.09	0.7040	0.0035	0.513723	0.000008
Omp.1	0.91	3.51	0.1568	0.0008	0.512905	0.000008
Omp.2	0.78	2.86	0.1654	0.0008	0.512911	0.000010
WR.Bomb	9.34	41.6	0.1359	0.0007	0.512891	0.000008
WR.Sav	9.15	40.7	0.1358	0.0007	0.512872	0.000007

^a WR.Bomb-whole rock by bomb digestion; WR.Sav-whole rock by table top digestion; Grt-garnet, Omp-omphacite.

[†] Reported errors on the ¹⁷⁶Hf/¹⁷⁷Hf and ¹⁴³Nd/¹⁴⁴Nd are within-run 2σ, standard error. Errors calculated for ages (not shown) are based on external reproducibility of spiked whole-rock samples (¹⁷⁶Hf/¹⁷⁷Hf = 0.01%, ¹⁴³Nd/¹⁴⁴Nd = 0.0035%) and within run errors (as reported above) added in quadrature.

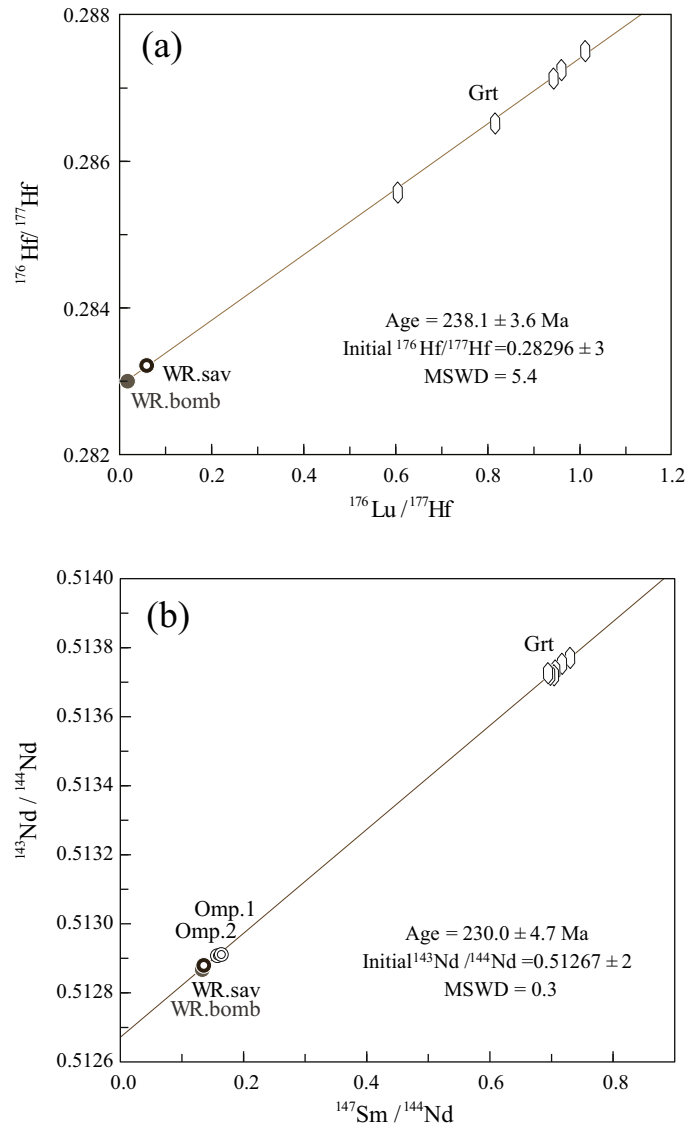


Fig. 8. Lu-Hf and Sm-Nd isochron plots for garnet fraction, bulk-rock powder and/or omphacite separate of the Bailang eclogite. Grt – garnet, Omp – omphacite, WR.sav – whole rock by Savillex-digestion, WR.bomb – whole rock by Bomb-digestion. Error bars are significantly smaller than the size of the symbols. MSWD – mean square of weighted deviates.

geochronometers. Diffusional decoupling between Lu-Hf and Sm-Nd would require long-term high temperatures and diffusion for a prolonged time to reset the two systems. Such a long-term high-

temperature history would have ultimately smooth major elemental zoning of the garnets, which was not observed in our sample. Garnet resorption could, plausibly, have affected the Sm-Nd age, as has been

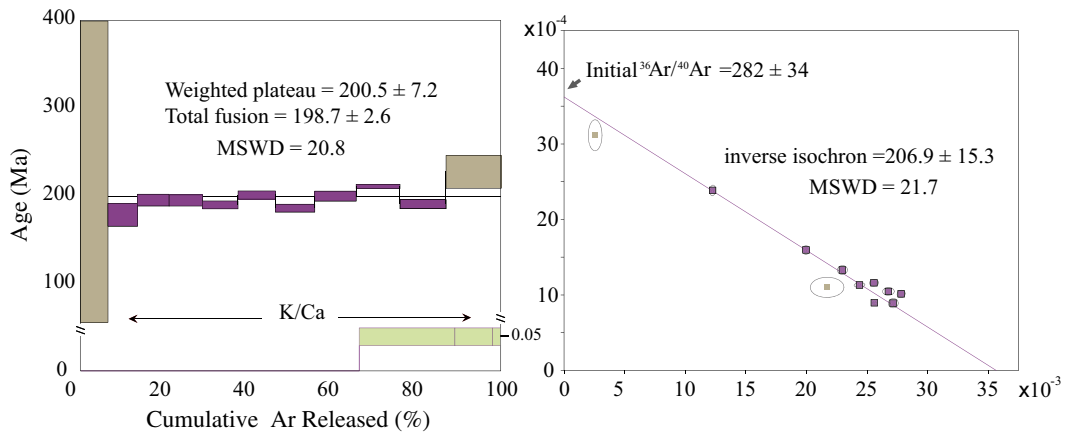


Fig. 9. $^{40}\text{Ar}/^{39}\text{Ar}$ data for the amphibole from the Bailang eclogite.

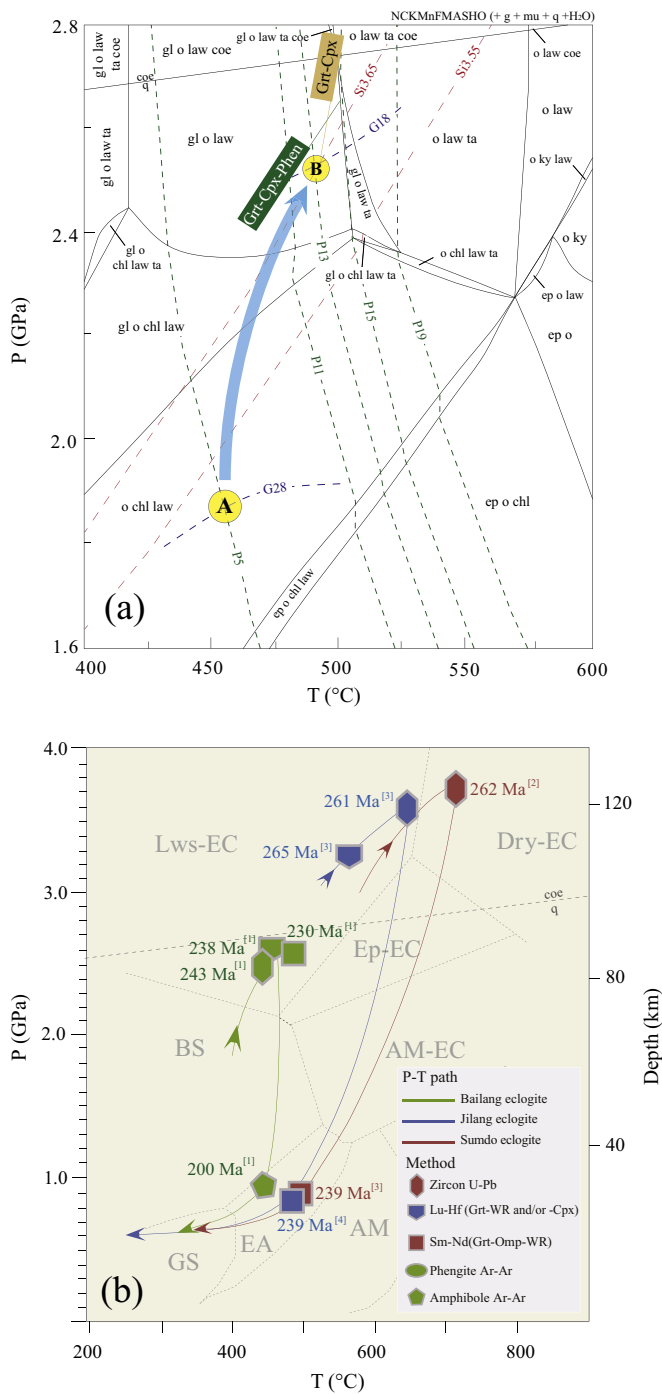


Fig. 10. (a) Estimated P - T conditions for the Bailang eclogite using the geothermobarometry of Krogh-Ravna (2000) and Krogh-Ravna and Terry (2004). P - T pseudosection calculated for the peak condition stage in the NCKMnFMASHO system using the Perple_X thermodynamic software (version 6.6.9; Connolly, 2005) using an effect bulk composition obtained by subtracting garnet core from the XRF-based bulk composition in supplemental materials, normalized on the basis of mole per cent as $\text{SiO}_2 = 56.29$, $\text{Al}_2\text{O}_3 = 9.13$, $\text{CaO} = 10.27$, $\text{MgO} = 9.99$, $\text{FeO} = 9.51$, $\text{K}_2\text{O} = 0.67$, $\text{Na}_2\text{O} = 3.53$, $\text{MnO} = 0.04$, $\text{O}_2 = 0.57$. The pseudosection was contoured with isopleths of grossular (e.g., G18) and pyrope (e.g., P13) contents in garnet, Si content in phengite (e.g., S13.48). (b) Schematic P - T - t paths for metamorphic processes of eclogites in the Lhasa terrane. The transition of quartz and coesite was calculated using Perple_X and the internally consistent thermodynamic data set of Holland and Powell (1998). Mineral abbreviations used are: chl, chlorite; coe, coesite; ep, epidote; gl, glaucophane; g, garnet; ky, kyanite; law, lawsonite; mu, phengitic muscovite; o, omphacite; q, quartz; ru, rutile. P - T boundaries of various metamorphic facies are indicated: GR, granulite, AM, amphibolite, EA, epidote amphibolite, BS, blueschist schist, GS, greenschist. The subdivisions of eclogite (EC) of amphibole eclogite (Amp-EC), epidote eclogite (Ep-EC), lawsonite eclogite (Lws-EC) and dry eclogite are also indicated. The P - T data are from Yang et al. (2009), Zhang et al. (2011) and Cheng et al. (2012). Reference: 1 = this study, 2 = Yang et al. (2009), 3 = Li et al. (2007), 4 = Li et al. (2011).

reported for the Lu-Hf system (Kelly et al., 2011). Subsequent retrograde dissolution could be evidenced by the observation of increasing spessartine at the garnet rims, which is not present in our sample (Fig. 5).

The tabletop digestion technique (Cheng et al., 2008) used in this study dissolves garnet completely and typically leaves zircon largely intact. Zircon, can potentially affect the apparent garnet age if not in isotopic equilibrium with the sample at the time of garnet formation and if present as inclusions in either the garnet or rock matrix (Scherer et al., 2000). The tabletop digestion technique makes the Lu-Hf technique much less susceptible to the presence of zircon inclusions. The consistency of the bulk and in situ Hf concentrations of the garnet fractions suggests that the selective digestion was effective in eliminating the contributions from zircon inclusions. Sm-Nd geochronology is sensitive to monazite and apatite inclusions, in which apatite is present as inclusions in our sample. Concentrations of Nd (0.4–1.8 ppm) and Sm/Nd ratios of 0.9–3.0 across single garnet, are consistent with those obtained by bulk isotopic digestion (Table 4), indicating that the Nd isotopic analyses in this study are essentially unaffected by MREE-rich inclusions. The Sm-Nd age represents average ages of all growth zones weighted by their respective Sm contents, which increased slightly towards the rim (Fig. 5). Thus, the Sm-Nd age likely skews towards later garnet growth because a much greater proportion of Sm is present within the outer shells, compared to the low-volume garnet core, i.e., the spherical geometry effect (Cheng et al., 2009). The Sm-Nd isochron age of 230.0 ± 4.7 Ma, including all garnet fragments, is thus interpreted to reflect the main episode of garnet growth, probably skewing to a later garnet growth episode.

The spread in parent/daughter ratios for the garnet segments, and the best-fit multi-fraction Lu-Hf isochron ($\text{MSWD} = 5.4$) out of a strict statistical sense ($\text{MSWD} = 2.2$ for 7-points or 6 degrees of freedom; Wendt and Carl, 1991), imply age differences for different portions of the garnet are beyond the analytical uncertainties (Kohn, 2009). The relatively large uncertainty of the isochron age evidently indicates involvement of diverse proportions of older core and younger rim material in the bulk isotopic digestion, which is consistent with the observation of the higher Lu content (~ 1.0 ppm) obtained by isotopic digestion than those of the garnet rim (~ 0.6 ppm). Combined with the strongly Rayleigh-like zoned HREE in garnet, the Lu-Hf age of 238.1 ± 3.6 Ma is thus interpreted to approximate the growth age of the garnet grains, skewing towards early garnet growth.

7.2.3. Amphibole Ar-Ar

On the inverse isochron diagram of $^{36}\text{Ar}/^{40}\text{Ar}$ vs $^{39}\text{Ar}/^{40}\text{Ar}$, the initial $^{40}\text{Ar}/^{36}\text{Ar}$ ratio of 282 ± 34 is comparable to the present day atmospheric composition of Ar. We thus conclude that no significantly excess Ar has been incorporated at or after the time of initial closure of the isotopic system in these amphibole. Therefore, the integrated age is interpreted to be geologically significant. Our estimate of the maximum temperature for the sample equals or exceeds the likely Ar closure temperature of $\sim 450 \pm 50$ °C for amphibole (Baldwin, 1996). Accordingly, we interpret the age as a minimum time estimate of the epidote-amphibolite metamorphism, and as dating cooling along a counter-clockwise P - T path from the early eclogite-amphibolite facies into blueschist-facies conditions. The ca. 200 Ma hornblende Ar-Ar age is coincided with the that of the ca. 210–190 Ma intrusion age of the granite that extended approximate 1400 km W-E in the Lhasa terrane (e.g., Li et al., 2003; Liu et al., 2006; Zhang et al., 2007), probably indicating related eclogite exhumation and the post-orogenic extension and granite activities.

7.3. Tectonic implications

7.3.1. Tectonic setting of the eclogite protolith

Deciphering the tectonic setting of a basaltic protolith is highly contentious and has been proved to be difficult (e.g., Bebout, 2007).

However, if one accepts that there are no significant changes in the 'immobile elements' abundances, such as HFSE and HREE, during subduction-zone metamorphism as illustrated by previous studies on mafic rocks from world-wide HP/UHP terranes (such as New Caledonia, Western Alps and Dabie-Sulu terranes; e.g., Becker et al., 2000; Spandler et al., 2003; Liu et al., 2008), we can use these immobile elements to help provide constraints on the initial tectonic setting of the protolith of the eclogite. In this scenario, several discrimination diagrams are used to help constrain the formation tectonic setting of the protolith Bailang eclogite.

The major and trace element compositions of the Bailang eclogite have high TiO_2 contents (>3%) and similar ranges of variation of REEs, resembling the patterns for enriched basalts of near-ridge seamounts or ocean island basalt (OIB) (Sun and McDonough, 1989). The Bailang eclogites are characterized by low Zr/Nb (7.1–11.7) and Y/Zr (0.13–0.20) ratios, high Nb concentrations (20.5–31.8 ppm), and high Th/Yb and Nb/Yb ratios, indicating that they were derived from an enriched mantle source similar to that for OIBs (Becker et al., 2000; Spandler et al., 2004). The OIB affinity for the samples are also suggested by their plotting in the OIB fields in the diagrams such as Ti vs V (Shervais, 1982; Fig. 11a), FeO/MgO vs TiO_2 (Glassiey, 1974; Fig. 11b), and Al_2O_3 vs TiO_2 (Spandler et al., 2004; Fig. 11c) diagrams.

In addition, the highly radiogenic initial Nd and Hf isotope compositions ($\epsilon_{\text{Nd}(0)}$ values of +5.1 and $\epsilon_{\text{Hf}(0)}$ values of $\sim +13.6$) suggest a juvenile crustal origin for the Bailang eclogite.

The Sumdo eclogite belt is a tectonic complex composed of metabasaltic rocks (blueschist and eclogite), ophiolitic mélange, OIB-type basalt, metapelite, and ultramafic rocks (Chen, 2010). Previous geochemical data indicate that the eclogites, such as the Sumdo and Jilang eclogites, are of typical N-MORB origin (Li et al., 2009). The N-MORB affinity of the eclogites may suggest the existence of a mid-ocean spreading ridge. The association of N-MORB and OIB affinity, however, may indicate a back-arc basin origin for these eclogites, because the volcanism of back-arc basin generates both MORB- and OIB-type basalts without subduction-related geochemical characteristics (Pearce et al., 1999).

Regardless of these particular settings, the eclogites reflect a fossil oceanic (sea-crustal) subduction at a convergent plate margin (Yang et al., 2009; Chen, 2010) followed by the ultimate closure of a part of the Paleo-Tethys Ocean or a back-arc basin.

7.3.2. The closure timing of the Paleo-Tethys Ocean in the Lhasa terrane

The MORB- and OIB-like eclogites in the Lhasa terrane underwent metamorphism in LT/HP conditions (Yang et al., 2006; Chen et al., 2007; Liu et al., 2009b; Yang et al., 2009; Zeng et al., 2009; Zhang et al., 2011; Cheng et al., 2012; this study), but with a low geothermal gradient of <10 °C/km (Fig. 10b), which is typical of the oceanic subduction zone. These eclogites are interpreted to be the remnants of the Paleo-Tethyan oceanic/seafloor crust. The eclogites, along with Permian island arc volcanic rocks to the north (Yang et al., 2009; Chen et al., 2010), are thus believed to mark a Carboniferous–Permian suture zone. Therefore, the Lhasa eclogite reflect oceanic/seafloor crustal subduction rather than continental subduction. This is similar to the UHP eclogites from the Limousin area in the Variscan French Massif Central (Berger et al., 2010) but quite unusual for most UHP rocks, especially those having a continental origin (c.f., Zheng, 2012).

U–Pb zircon ages of 262 ± 5 Ma and 261 ± 3 Ma were obtained for the Sumdo eclogite (Yang et al., 2009) and the Jilang eclogite (Cheng et al., 2012), respectively. These ages were interpreted to reflect eclogite-facies metamorphism, and are comparable to the Lu–Hf isochron age of 265.9 ± 1.1 Ma for the Jilang eclogite (Cheng et al., 2012). U–Pb zircon ages of ca. 290 Ma were obtained for both the Jilang eclogite and the quartzite (Cheng et al., 2012), which are comparable to the 285–303 Ma U–Pb zircon age for the OIB-like basalts from Xindalang Country (Chen, 2010) and the 287–292 Ma U–Pb ages of the magmatic zircons from the Sumdo and Jilang eclogites (Yang et al., 2009; Cheng

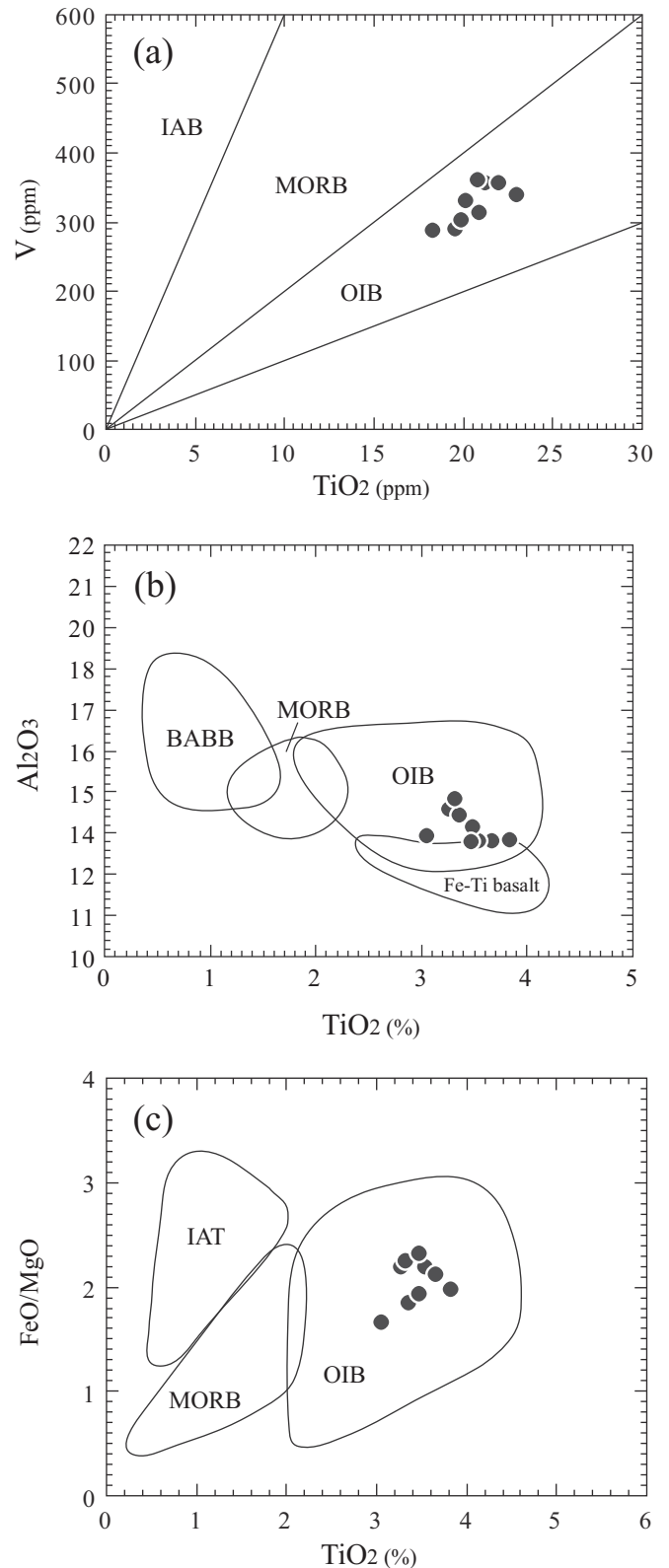


Fig. 11. Ti vs V (Shervais, 1982), FeO/MgO vs TiO_2 (Glassiey, 1974), and Al_2O_3 vs TiO_2 (Spandler et al., 2004) diagrams for the Bailang eclogite. IAT – island arc tholeiitic basalt; BABB – back-arc basin basalt; OIB – oceanic island basalt; IAB – island arc basalt; MORB – middle ocean ridge basalt.

et al., 2012). The latter ages were believed to represent the protolith age of the eclogites. Therefore, the initiation of the opening the oceanic basin in the Lhasa terrane was no later than ca. 290 Ma. This HP/UHP

eclogite belt, together with the northern Carboniferous to Permian island arc volcanic rocks, Permian peraluminous granite (*ca.* 263 Ma) and the regional angular unconformity between the Middle and the Upper Permian, could be related to an Andean-type orogeny that likely resulted from the northward subduction of the Paleo-Tethys oceanic crust beneath the North Lhasa terrane (Yang et al., 2009; Zhu et al., 2011; Cheng et al., 2012) prior to *ca.* 266 Ma.

The Sm–Nd age of 230.0 ± 4.7 Ma for the Bailang eclogite (Fig. 8) reflects eclogite-facies metamorphism, and is significant younger than the eclogite-facies metamorphic age of *ca.* 266 Ma for the zircons of the Sumdo and Jilang eclogites, but coincidentally resembling the cooling ages of these eclogites. Our new ages, combined with the existing geochronologic data set for Lhasa eclogites, suggest that the (U)HP metamorphism of the Lhasa terrane occurred over ~ 30 Myr period. These eclogite ages come from a small portion of the Lhasa terrane, spanning 10 km north to south and 30 km west toward east.

If the entire area subducted as a coherent block, this would require a long-term residence (~ 30 Myr) of a $\sim 30 \times 10$ km² piece of subducted oceanic crust at great depth which seems implausible. To a first order approximation, this would require very slow subduction rate (less than 1.0 mm/yr) significantly slower than the average rate of Andean style subduction zones (Jarrard, 2003; Lallemand et al., 2005). Moreover, subducted oceanic crust would not survive such long residence in the hot mantle without melting (Root et al., 2005), assuming a thermal diffusivity of 10^{-6} m²/s (Turcotte and Schubert, 2002). Furthermore, the zoned major elemental profiles of garnet allow for an estimate of the maximum interval of diffusive homogenization. As a first approximation, the following calculations assume that the volume diffusion of elements is the rate-limiting factor for chemical homogenization and for a spherical geometry for garnets. This approximation is carried on the earlier (older age) subducted eclogite, i.e., the Sumdo and Jilang eclogites (Yang et al., 2009; Cheng et al., 2012). The time-scale required for complete homogenization of a garnet grain is given by the relationship $r = 2.5 \times (Dt)^{1/2}$ (Crank, 1983), where r is the effective diffusion radius, D is the diffusion coefficient (Chakraborty and Ganguly, 1992) and t is the time. Given a temperature of 650–700 °C, a duration of ~ 0.4 – 5.6 Myr is required for Mg–Mn–Ca to be completely homogenized by

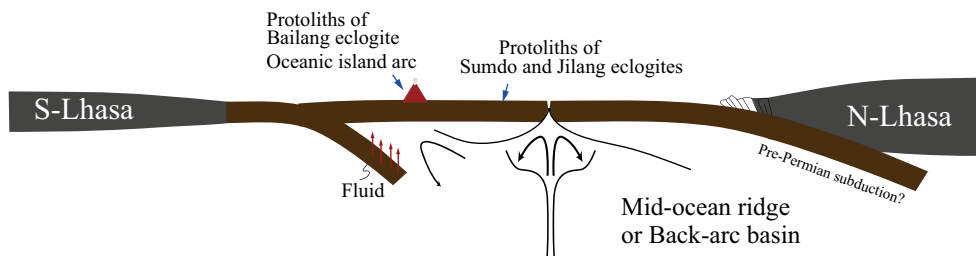
diffusion across the garnet core–mantle portion (~ 0.5 mm in radius). The partially preserved Mg, Fe and Mn zoning (Yang et al., 2009; Cheng et al., 2012) indicates that they have not experienced long residence ($> \sim 6$ Ma) at high temperature. Long-term metamorphism under (U)HP conditions is therefore an unlikely mechanism for the large span of ages for eclogites in the Lhasa terrane.

The number of recognized UHP rocks worldwide has increased dramatically in the last thirty years. Recently, increasing evidences from the study of orogens worldwide indicate different HP and UHP slices within a single orogeny have undergone different subduction and exhumation histories (e.g., Xu et al., 2006; Liu et al., 2009a; Herwartz et al., 2011; Liu et al., 2011; Lanari et al., 2012). The eclogites from the Lhasa terrane record a wide range of peak metamorphic conditions, from ~ 450 to ~ 790 °C at about 2.5 GPa to 3.9 GPa at a time span from *ca.* 266 Ma to *ca.* 238 Ma. This, together with their intimate occurrence indicates that they cannot belong to one coherent block but, rather, distinct slices that were derived from different depths at different times in the subduction zone that were subsequently juxtaposed. A diachronous subduction model for the evolution of the Lhasa eclogite is thus proposed (Fig. 12). The initiation of the opening the Paleo-Tethys Ocean in the Lhasa terrane could trace back to the Early Permian. Based on the diverse P – T – t trajectories of the Lhasa eclogite, the Paleo-Tethys oceanic/sea-floor crust can be classified into a UHP crustal slice I (enclosing Jilang and Sumdo eclogites) and an HP crustal slice II (hosting Bailang eclogites). The eclogites were formed during the closure of the Paleo-Tethys Ocean, which initiated prior to *ca.* 266 Ma. Slice I was detached from the down-going slabs and subsequently exhumed at *ca.* 240 Ma; slice II initiated subduction and did not reach the ultimate depth until *ca.* 230 Ma before detachment and significant exhumation at *ca.* 200 Ma (Fig. 12). The ultimate closure of the Paleo-Tethys Ocean in the Lhasa terrane was no earlier than *ca.* 230 Ma.

7.3.3. Tectonic model of evolution of the Lhasa terrane

Various models have been proposed for the origin and evolution of the Himalayan–Tibetan orogen resulting from several collisional events among a series of Gondwana-derived terranes (e.g., Qiangtang, Lhasa and India) and the Asian continent since the early Paleozoic

(a) Formation of the protolith of Lhasa eclogites (Carboniferous–Permian)



(b) Subduction of the Lhasa eclogites (Permian–Triassic)

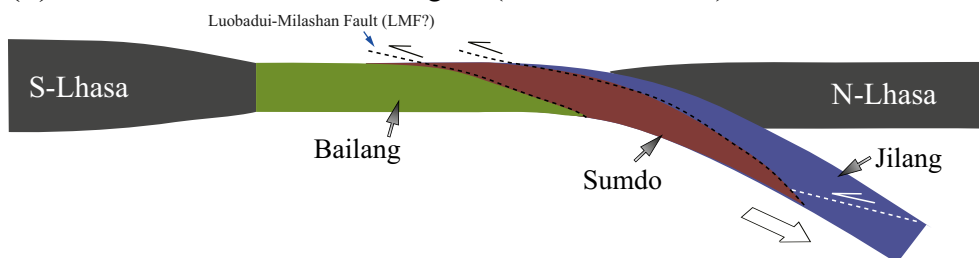


Fig. 12. Tectonic model for the eclogites from the Lhasa terrane; (a) formation of eclogite protolith during Carboniferous to Permian; (b) diachronous subduction of the Paleo-Tethy Ocean during Permian to Triassic.

(e.g., Metcalfe, 1996; Şengör and Natalin, 1996; Yin and Harrison, 2000; Gehrels et al., 2011; Zhu et al., 2013; Zhang et al., 2014a; Zhang et al., 2014b). The Lhasa terrane occupies an important position in the Himalayan–Tibetan orogen, and therefore the origin and evolutionary history of this terrane is the key for understanding the tectonic models on this orogen. Zhang et al. (2014a) and Zhang et al. (2014b) suggested that the Lhasa terrane experienced multistage and multiple metamorphic events from the Neoproterozoic to Cenozoic. The temporal and spatial evolution of metamorphic processes and their geodynamics can provide independent means to reconstruct the geological history of the Lhasa terrane and the Himalayan–Tibetan orogen, and also to evaluate the previous models which are mostly based on magmatic, paleomagnetic, and paleogeographic data (Zhang et al., 2014a; Zhang et al., 2014b).

Proposing a tectonic model to explain the origin and evolution of the entire Lhasa terrane is far beyond current study. Nevertheless, our data have confirmed a Late Permian HP metamorphic belt, represented by the Lhasa eclogite, that occurs between the South and North Lhasa terranes (Xu et al., 2007; Chen et al., 2009; Liu et al., 2009b; Yang et al., 2009; Zeng et al., 2009). This stage of metamorphism occurred under LT/HP conditions, with a low geothermal gradient of <10 °C/km (Fig. 5), which is consistent with the presence of lawsonite inclusion in garnet from the Bailang eclogite and typical of the oceanic subduction zone. Thus, this HP belt, together with the northern Carboniferous to Permian island arc volcanic rocks, Permian peraluminous granite and the regional angular unconformity between the Middle and the Upper Permian, appear to be related to an Andean-type orogeny that probably resulted from the northward subduction of the Paleo-Tethys beneath the North Lhasa terrane (Yang et al., 2009; Zeng et al., 2009; Zhu et al., 2011). Previous studies suggest a middle pressure metamorphic belt with a length of up to 500 km is present between the South and North Lhasa terranes (Dong et al., 2011; Zhang et al., 2014a; Zhang et al., 2014b). Zircon U–Pb dating on the amphibolite, schist, and gneiss, indicates that these rocks were metamorphosed during 225–210 Ma (Dong et al., 2011; Zhang et al., 2014a; Zhang et al., 2014b). This Triassic MP metamorphism is associated with widespread granitic magmatism with a geochemical affinity to that of the syn- or post-collisional plutons (Li et al., 2003; Kapp et al., 2005; Zhang et al., 2007; Zhu et al., 2011). Collectively, following the closure of the Paleo-Tethys Ocean at ca. 230 Ma, the collision of the South and North Lhasa terranes built an extensive Triassic epidote-amphibolite- to amphibolite-facies metamorphic belt (Dong et al., 2011; Zhang et al., 2014a; Zhang et al., 2014b) with an E–W extension of at least 500 km and the coeval granitic magmatism with a geochemical affinity to that of the syn- or post-collisional plutons (Li et al., 2003; Booth et al., 2004; Kapp et al., 2005) across the Lhasa terrane.

8. Conclusions

Combined geochemical and geochronological data of the Bailang eclogite from the Lhasa terrane suggest:

- (1) The protolith of the Bailang eclogite is of an OIB affinity.
- (2) The Lhasa (U)HP metamorphic belt comprises different slices that had distinct P – T histories and hence underwent (U)HP metamorphism at different times.
- (3) The opening of the Paleo-Tethys Ocean in the Lhasa terrane initiated prior to ca. 266 Ma and its ultimate closure was no earlier than ca. 230 Ma.

Acknowledgements

This material was based upon work supported by the National Natural Science Foundation of China (41373005). We thank D. Wilford, C. Zhang and C. Knaack at Pullman for their assistance with isotope geochemistry and mass spectrometry respectively. We thank Z.M. Zhang and M. Santosh for their carefully editorial managing of the manuscript.

Two anonymous reviewer and Z.M. Zhang are thanked for their insightful comments that greatly improved the clarity and content of the manuscript.

Appendix A. Supplementary data

Supplementary data to this article can be found online at <http://dx.doi.org/10.1016/j.gr.2014.09.017>.

References

- Baldwin, S.L., 1996. Contrasting P – T histories for blueschists from the Western Baja terrane and the Aegean: Effects of syn-subduction exhumation and backarc extension. In: Bebout, E.G., Scholl, D.W., Kirby, S.H., Platt, J.P. (Eds.), Subduction top to bottom. Geophysical Monograph 96, pp. 35–141.
- Bebout, G.E., 2007. Metamorphic chemical geodynamics of subduction zones. *Earth and Planetary Science Letters* 260, 373–393.
- Becker, H., Jochum, K.P., Carlson, R.W., 2000. Trace element fractionation during dehydration of eclogites from high-pressure terranes and the implications for element fluxes in subduction zones. *Chemical Geology* 163, 65–99.
- Berger, J., Féménias, O., Ohnenstetter, D., Bruguier, O., Plissart, G., Mercier, J.C.C., Demaiffe, D., 2010. New occurrence of UHP eclogites in Limousin (French Massif Central): age, tectonic setting and fluid–rock interactions. *Lithos* 118, 365–382.
- Berman, R.G., 1988. Internally-consistent thermodynamic data for minerals in the system Na_2O – K_2O – CaO – MgO – FeO – Fe_2O_3 – Al_2O_3 – SiO_2 – TiO_2 – H_2O – CO_2 . *Journal of Petrology* 29, 445–522.
- BGMXRAR (Bureau of Geology Mineral Resources of Xizang Autonomous Region), 1993. Regional Geology of Xizang (Tibet) Autonomous Region. Geological Publishing House, Beijing, pp. 1–450 (in Chinese with English abstract).
- Bloch, E., Ganguly, J., Hervig, R., 2010. Diffusion kinetics of hafnium in garnet: Experimental determination and geochronological implications. *Goldschmidt Conference abstract A97*.
- Booth, A.L., Zeitler, P.K., Kidd, W.S.F., Wooden, J., Liu, Y.P., Idleman, B., Hren, M., Chamberlain, C.P., 2004. U–Pb zircon constraints on the tectonic evolution of Southeastern Tibet, Namche Barwa area. *American Journal of Science* 304, 889–929.
- Bouvier, A., Vervoort, J.D., Patchett, P.J., 2008. The Lu–Hf and Sm–Nd isotopic composition of CHUR: constraints from unequilibrated chondrites and implications for the bulk composition of terrestrial planets. *Earth and Planetary Science Letters* 273, 48–57.
- Carlson, W.D., 2012. Rates and mechanisms of Y, REE, and Cr diffusion in garnet. *American Mineralogist* 97, 1598–1618.
- Chakraborty, S., Ganguly, J., 1992. Cation diffusion in aluminosilicate garnets: Experimental determination in spessartine–almandine diffusion couples, evaluation of effective binary diffusion coefficients and applications. *Contributions to Mineralogy and Petrology* 111, 74–86.
- Chen, S.Y., 2010. The development of Sumdo suture in the Lhasa Block, Tibet (Ph.D. Thesis) Chinese Academy of Geological Science, Beijing, p. 199 (in Chinese with English abstract).
- Chen, S.Y., Yang, J.S., Luo, L.Q., Li, Z.L., Xu, X.Z., Li, T.F., Ren, Y.F., Li, H.Q., 2007. MORB-type eclogites in the Lhasa block, Tibet, China: petrochemical evidence. *Geological Bulletin of China* 26, 1327–1339.
- Chen, S.Y., Yang, J.S., Li, Y., Xu, X.Z., 2009. Ultramafic blocks in Sumdo region, Lhasa Block, eastern Tibet Plateau: an ophiolite unit. *Journal of Earth Science* 20, 332–347.
- Chen, J.S., Huang, B.C., Sun, L.S., 2010. New constraints to the onset of the India–Asia collision: paleomagnetic reconnaissance on the Linzizong Group in the Lhasa Block, China. *Tectonophysics* 489 (2010), 189–209.
- Chen, Y., Zhang, Z.J., Sun, C.Q., Badal, J., 2013. Crustal anisotropy from Moho converted Ps wave splitting analysis and geodynamic implications beneath the eastern margin of Tibet and surrounding regions. *Gondwana Research* 24, 946–957.
- Cheng, H., King, R.L., Nakamura, E., Vervoort, J.D., Zhou, Z., 2008. Coupled Lu–Hf and Sm–Nd geochronology constrains garnet growth in ultra-high-pressure eclogites from the Dabie orogen. *Journal of Metamorphic Geology* 26, 741–758.
- Cheng, H., King, R.L., Nakamura, E., Vervoort, J.D., Zheng, Y.F., Ota, T., Wu, Y.B., Kobayashi, K., Zhou, Z.Y., 2009. Transitional time of oceanic to continental subduction in the Dabie orogen: constraints from U–Pb, Lu–Hf, Sm–Nd and Ar–Ar multichronometric dating. *Lithos* 101, 327–342.
- Cheng, H., Zhang, C., Vervoort, D.J., Wu, Y.B., Zheng, Y.F., Zheng, S., Zhou, Z.Y., 2011. New Lu–Hf geochronology constrains the onset of continental subduction in the Dabie orogen. *Lithos* 121, 41–54.
- Cheng, H., Zhang, C., Vervoort, J.D., Lu, H.H., Wang, C., Cao, D.D., 2012. Zircon U–Pb and garnet Lu–Hf geochronology of eclogites from the Lhasa Block, Tibet. *Lithos* 155, 341–359.
- Connolly, J.A.D., 2005. Computation of phase equilibria by linear programming: a tool for geodynamic modeling and its application to subduction zone decarbonation. *Earth and Planetary Science Letters* 236, 524–541.
- Corfu, F., Hancher, J.M., Hoskin, P.W.O., Kinny, P., 2003. Atlas of zircon textures. *Reviews in Mineralogy and Geochemistry* 53, 469–500.
- Coulon, C., Maluski, H., Bollinger, C., Wang, S., 1986. Mesozoic and Cenozoic volcanic rocks from central and southern Tibet: $^{39}\text{Ar}/^{40}\text{Ar}$ dating, petrological characteristics and geodynamical significance. *Earth and Planetary Science Letters* 79, 281–302.
- Crank, J., 1983. *The mathematics of diffusion*, 2nd ed. Oxford University Press, Oxford.
- Diener, J.F.A., Powell, R., 2012. Revised activity–composition models for clinopyroxene and amphibole. *Journal of Metamorphic Geology* 30, 113–234.

- Ding, H.X., Zhang, Z.M., Dong, X., Yan, R., Lin, Y.H., Jiang, H.Y., 2015. Cambrian ultrapotassic rhyolites from the Lhasa terrane, south Tibet: Evidence for Andean-type magmatism along the northern active margin of Gondwana. *Gondwana Research* 27, 1616–1629.
- Dodson, M.H., 1973. Closure temperature in cooling geochronological and petrological systems. *Contributions to Mineralogy and Petrology* 40, 259–274.
- Dong, X., Zhang, Z.M., Liu, F., Wang, W., Yu, F., Shen, K., 2011. Zircon U–Pb geochronology of the Nyainqêntanglha Group from the Lhasa terrane: new constraints on the Triassic orogeny of the south Tibet. *Journal of Asian Earth Sciences* 42, 723–739.
- Evans, T.P., 2004. A method for calculating effective bulk composition modification due to crystal fractionation in garnet-bearing schist: implications for isopleth thermobarometry. *Journal of Metamorphic Geology* 22, 547–557.
- Ferrari, O.M., Hochard, C., Stampfli, G.M., 2008. An alternative plate tectonic model for the Palaeozoic–Early Mesozoic Palaeotethyan evolution of Southeast Asia (Northern Thailand–Burma). *Tectonophysics* 451, 346–365.
- Ganguly, J., Tirone, M., Hervig, R., 1998. Diffusion kinetics of Samarium and Neodymium in garnet, and a method for determining cooling rates of rocks. *Science* 281, 805–807.
- Ganguly, J., Bloch, E., Ito, M., 2011. Experimental diffusion kinetics of geochronological systems and interpretations of mineral ages in terrestrial rocks and meteorites. *GSA Denver Annual Meeting*, Paper no. 135–2.
- Gehrels, G., Kapp, P., DeCelles, P., Pullen, A., Blakey, R., Weislogel, A., Ding, L., Guynn, J., Martin, A., McQuarrie, N., Yin, A., 2011. Detrital zircon geochronology of Pre-Tertiary strata in the Tibetan–Himalayan orogen. *Tectonics* 30, TC5016. <http://dx.doi.org/10.1029/2011TC002868>.
- Girardeau, J., Marcoux, J., Fourcade, E., Bassoulet, J.P., Tang, Y.K., 1985. Xainxa ultramafic rocks, central Tibet, China: tectonic environment and geodynamic significance. *Geology* 13, 330–333.
- Glassiey, W., 1974. *Geochemistry and tectonics of Gressent volcanic rocks, Olympia Peninsula, Washington*. Geological Society of America Bulletin 85, 785–794.
- Green, T.H., Blundy, J.D., Adam, J., Xaxley, G.M., 2000. SIMS determination of trace element partition coefficients between garnet, clinopyroxene and hydrous basaltic liquids at 2–7.5 GPa and 1080–1200 °C. *Lithos* 53, 165–187.
- Guynn, J., Kapp, P., Gehrels, G., Ding, L., 2012. U–Pb geochronology of basement rocks in central Tibet and paleogeographic implications. *Journal of Asian Earth Sciences* 43, 23–50.
- Hanchar, J.M., Hoskin, P.W.O., 2003. Zircon. *Reviews in Mineralogy and Geochemistry* 53, 1–500.
- Hébert, R., Bezard, R., Guilmette, C., Dostal, J., Wang, C.S., Liu, Z.F., 2012. The Indus–Yarlung Zangbo ophiolites from Nanga Parbat to Namche Barwa syntaxes, southern Tibet: first synthesis of petrology, geochemistry, and geochronology with incidences on geodynamic reconstructions of Neo-Tethys. *Gondwana Research* 22, 377–397.
- Hébert, R., Guilmette, C., Dostal, J., Bezard, R., Lesage, G., Bédard, É., Wang, C.S., 2014. Miocene post-collisional shoshonites and their crustal xenoliths, Yarlung Zangbo Suture Zone southern Tibet: Geodynamic implications. *Gondwana Research* 25, 1263–1271.
- Herwartz, D., Nagel, T.J., Munker, C., Scherer, E.E., Froitzheim, N., 2011. Tracing two orogenic cycles in one eclogite sample by Lu–Hf garnet chronometry. *Nature Geoscience* 4, 178–183.
- Holland, T.J.B., Powell, R., 1998. An internally consistent thermodynamic data set for phases of petrological interest. *Journal of Metamorphic Geology* 16, 309–343.
- Hollister, L.S., 1966. Garnet zoning: an interpretation based on the Rayleigh fractionation model. *Science* 154, 1647–1651.
- Hoskin, P.W.O., 2005. Trace-element composition of hydrothermal zircon and the alteration of Hadean zircon from the Jack Hills, Australia. *Geochimica et Cosmochimica Acta* 69, 637–648.
- Hoskin, P.W.O., Black, L.P., 2000. Metamorphic zircon formation by solid state recrystallization of protolith igneous zircon. *Journal of Metamorphic Geology* 18, 423–439.
- Hsü, K.J., Pan, G.T., Sengör, A.M.C., 1995. Tectonic evolution of the Tibetan Plateau: a working hypothesis based on the archipelago model of orogenesis. *International Geology Review* 37, 473–508.
- Jarrard, R.D., 2003. Subduction fluxes of water, carbon dioxide, chlorine, and potassium. *Geochemistry, Geophysics, Geosystems* 4, 8905. <http://dx.doi.org/10.1029/2002GC000392>.
- Kapp, J.L.D., Harrison, T.M., Kapp, P., Grove, M., Lovera, O.M., Lin, D., 2005. Nyainqêntanglha Shan: a window into the tectonic, thermal, and geochemical evolution of the Lhasa block, southern Tibet. *Journal of Geophysical Research – Solid Earth* 110. <http://dx.doi.org/10.1029/2004JB003330>.
- Kelly, E.D., Carlson, W.D., Connelly, J.N., 2011. Implications of garnet resorption for the Lu–Hf geochronometer: An example from the contact aureole of the Makhavinekh Lake Pluton, Labrador. *Journal of Metamorphic Geology* 29, 901–916.
- Klootwijk, C., 2013. Middle–Late Paleozoic Australia–Asia convergence and tectonic extrusion of Australia. *Gondwana Research* 24, 5–54.
- Kohn, M.J., 2009. Models of garnet differential geochronology. *Geochimica et Cosmochimica Acta* 73, 170–182.
- Koppers, A.A.P., 2002. ArArCALC-software for ⁴⁰Ar/³⁹Ar age calculations. *Computers and Geosciences* 28, 605–619.
- Krogh-Ravna, E.J.K., 2000. The garnet-clinopyroxene Fe²⁺–Mg geothermometer: an updated calibration. *Journal of Metamorphic Geology* 18, 21–219.
- Krogh-Ravna, E.J.K., Terry, M.P., 2004. Geothermobarometry of UHP and HP eclogites and schists – an evaluation of equilibria among garnet-clinopyroxene-kyanite-phengite-coesite/quartz. *Journal of Metamorphic Geology* 22, 579–592.
- Lallemant, S., Heuret, A., Boutelier, D., 2005. On the relationships between slab dip, back-arc stress, upper plate absolute motion, and crustal nature in subduction zones. *Geochemistry, Geophysics, Geosystems* 6 (9), Q09006. <http://dx.doi.org/10.1029/2005GC000917>.
- Lanari, P., Guillot, S., Schwartz, S., Vidal, O., Tricart, P., Riel, N., Beyssac, O., 2012. Diachronous evolution of the alpine continental subduction wedge: evidences from P–T estimates in the Briançonnais Zone houillère (France–Western Alps). *Journal of Geodynamics* 56–57, 39–54.
- Lapen, T.J., Johnson, C.M., Baumgartner, L.P., Mahlen, N.J., Beard, B.L., Amato, J.M., 2003. Burial rates during prograde metamorphism of an ultra-high-pressure terrane: An example from Lago di Cignana, western Alps, Italy. *Earth and Planetary Science Letters* 215, 57–72.
- Leake, B.A., Woolley, A.R., Arps, C.E.S., Birch, W.D., Gilbert, M.C., Grice, J.D., Hawthorne, F.C., Kato, A., Kisch, H.J., Krivovichev, V.G., Linthout, K., Laird, J., Mandarino, J., Maresch, W.V., Nickel, E., Rock, N.M.S., Schumacher, J.C., Smith, D.C., Stephenson, N.C.N., Ungaretti, L., Whittaker, E.J.W., Youzmi, G., 1997. Nomenclature of amphiboles. Report of the Subcommittee on Amphiboles of the International Mineralogical Association Commission on New Minerals and Mineral Names. *European Journal of Mineralogy* 9, 623–651.
- LeBas, M.J., 1989. Nephelinitic and basanitic rocks. *Journal of Petrology* 30, 1299–1312.
- Leeder, M.R., Smith, A.B., Yin, J.X., 1988. Sedimentology and palaeoenvironmental evolution of the 1985 Lhasa to Golmud Geotraverse. *Philosophical Transactions of the Royal Society of London Series A* 327, 107–143.
- Li, C., Wang, T.W., Li, H.M., Zeng, Q.G., 2003. Discovery of Indosinian megaporphyritic granodiorite in the Gangdise area: evidence for the existence of Paleo-Gangdise. *Geological Bulletin of China* 22, 364–366 (in Chinese with English abstract).
- Li, T.F., Yang, J.S., Li, Z.L., Xu, X.Z., Ren, Y.F., Wang, R.C., Zhang, W.L., 2007. Petrography and metamorphic evolution of the Sumdo eclogite, Qinghai–Tibetan Plateau. *Geological Bulletin of China* 26, 1310–1326 (in Chinese with English abstract).
- Li, Z.L., Yang, J.S., Xu, Z.Q., Li, T.F., Xu, X.Z., Ren, Y.F., Robinson, O.T., 2009. Geochemistry and Sm–Nd and Rb–Sr isotopic composition of eclogite in the Lhasa terrane, Tibet, and its geological significance. *Lithos* 109, 240–247.
- Li, H.Q., Xu, Z.Q., Yang, J.S., Tang, Z.M., Yang, M., 2011. Syn-collision exhumation of Sumdo eclogite in the Lhasa terrane, Tibet: Evidences from structural deformation and Ar–Ar geochronology. *Earth Science Frontiers* 18, 66–78 (in Chinese with English abstract).
- Li, G.W., Sandiford, M., Liu, X.H., Xu, Z.Q., Wei, L.J., Li, H.Q., 2014. Provenance of Late Triassic sediments in central Lhasa terrane, Tibet and its implication. *Gondwana Research* 25, 1680–1689.
- Liu, Q.S., Jiang, W., Jian, P., Ye, P.S., Wu, Z.H., Hu, D.G., 2006. Zircon SHRIMP U–Pb age and petrochemical and geochemical features of Mesozoic muscovite monzonitic granite at Ningzhong, Tibet. *Acta Petrologica Sinica* 22, 643–652 (in Chinese with English abstract).
- Liu, Y.S., Hu, Z.C., Gao, S., Günther, D., Xu, J., Gao, C.G., Chen, H.H., 2008. In situ analysis of major and trace elements of anhydrous minerals by LA-ICP-MS without applying an internal standard. *Chemical Geology* 257, 34–43.
- Liu, F.L., Gerdes, A., Xue, H.M., 2009a. Differential subduction and exhumation of crustal slices in the Sulu HP–UHP metamorphic terrane: insights from mineral inclusions, trace element, U–Pb and Lu–Hf isotope analyses of zircon in orthogneiss. *Journal of Metamorphic Geology* 27, 805–825.
- Liu, Y., Liu, H.F., Theye, T., Massonne, H.J., 2009b. Evidence for oceanic subduction at the NE Gondwana margin during Permo-Triassic times. *Terra Nova* 21, 195–202.
- Liu, F.L., Gerdes, A., Xue, H.M., 2011. Differential subduction and exhumation of crustal slices in the Sulu HP–UHP metamorphic terrane: insights from mineral inclusions, trace elements, U–Pb and Lu–Hf isotope analyses of zircon in orthogneiss. *Journal of Metamorphic Geology* 27, 805–825.
- Liu, Z., Jiang, Y.H., Jia, R.Y., Zhao, P., Zhou, Q., 2015. Origin of Late Triassic high-K calc-alkaline granitoids and their potassic microgranular enclaves from the western Tibet Plateau, northwest China: Implications for Paleo-Tethys evolution. *Gondwana Research* 27, 326–341.
- Lugmair, G.W., Marti, K., 1977. Sm–Nd–Pu timepieces in the Angra Dos Reis meteorite. *Earth and Planetary Science Letters* 35, 273–284.
- Metcalf, I., 1996. Gondwanaland dispersion, Asian accretion and evolution of Eastern Tethys. *Australian Journal of Earth Sciences* 43, 605–623.
- Mezger, K., Essene, E.J., Halliday, A.N., 1992. Closure temperatures of the Sm–Nd system in metamorphic garnets. *Earth and Planetary Science Letters* 113, 397–409.
- Morimoto, N., 1988. Nomenclature of pyroxenes. *Mineralogical Magazine* 52, 535–550.
- Nasdala, L., Hofmeister, W., Norberg, N., Mattinson, J.M., Corfu, F., Dörr, W., Kamo, S.L., Kennedy, A.K., Kronz, A., Reiners, P.W., Frei, D., Kosler, J., Wan, Y., Götze, J., Häger, T., Kröner, A., Valley, J.W., 2008. Zircon M257-A homogeneous natural reference material for the ion microprobe U–Pb analysis of zircon. *Geostandards and Geoanalytical Research* 32, 247–265.
- Pearce, J.A., Kempton, P.D., Nowell, G.M., Noble, S.R., 1999. Hf–Nd element and isotope perspective on the nature and provenance of mantle and subduction components in Western Pacific arc-basin system. *Journal of Petrology* 40, 1579–1611.
- Qiu, H.N., Wijbrans, J.R., 2006. Paleozoic ages and excess ⁴⁰Ar in garnets from the Bixiling eclogite in Dabieshan, China: new insights from ⁴⁰Ar/³⁹Ar dating by stepwise crushing. *Geochimica et Cosmochimica Acta* 70, 2354–2370.
- Ran, B., Wang, C.S., Zhao, X.X., Li, Y.L., He, M., Zhu, L.D., Coe, R.S., 2012. New paleomagnetic results of the early Permian in the Xainza area, Tibetan Plateau and their paleogeographical implications. *Gondwana Research* 22, 447–460.
- Rayner, N., Stern, R.A., Carr, S.D., 2005. Grain-scale variations in trace element composition of fluid-altered zircon, Acasta Gneiss Complex, northwestern Canada. *Contributions to Mineralogy and Petrology* 148, 721–734.
- Root, D.B., Hacker, B.R., Gans, P.B., Ducea, M.N., Eide, E.A., Mosenfelder, J.L., 2005. Discrete ultrahigh-pressure domains in the Western Gneiss region, Norway: implications for formation and exhumation. *Journal of Metamorphic Geology* 23, 45–61.
- Rubatto, D., 2002. Zircon trace element geochemistry: partitioning with garnet and the link between U–Pb ages and metamorphism. *Chemical Geology* 184, 123–138.
- Scherer, E.E., Cameron, K.L., Blichert-Toft, J., 2000. Lu–Hf garnet geochronology: Closure temperature relative to the Sm–Nd system and the effects of trace mineral inclusions. *Geochimica et Cosmochimica Acta* 64, 3413–3432.

- Scherer, E.E., Münker, C., Mezger, K., 2001. Calibration of the lutetium–hafnium clock. *Science* 293, 683–687.
- Schumacher, J.C., 1991. Empirical ferric iron corrections: necessity, assumptions and effects on selected geothermobarometers. *Mineral Magazine* 55, 3–18.
- Sengör, A.M.C., 1984. The Cimmeride orogenic system and the tectonics of Eurasia. *Geological Society of America, Special Paper* 195, 1–82.
- Şengör, A.M.C., Natalin, B.A., 1996. Paleotectonics of Asia: Fragments of a synthesis. In: Yin, A., Harrison, T.M. (Eds.), *The tectonic evolution of Asia*. Cambridge Univ. Press, New York, pp. 486–640.
- Shervais, J.W., 1982. Ti–V plots and the petrogenesis of modern and ophiolitic lavas. *Earth and Planetary Science Letters* 59, 101–118.
- Skora, S., Baumgartner, L.P., Mahlen, N.J., Johnson, C.M., Pilet, S., Hellebrand, E., 2006. Diffusion-limited REE uptake by eclogite garnets and its consequences for Lu–Hf and Sm–Nd geochronology. *Contributions to Mineralogy and Petrology* 152, 703–720.
- Smit, M.A., Scherer, E.E., Mezger, K., 2013. Lu–Hf and Sm–Nd garnet geochronology: Chronometric closure and implications for dating petrological processes. *Earth and Planetary Science Letters* 381, 222–233.
- Smye, A.J., Greenwood, L.V., Holland, T.J.B., 2010. Garnet–chloritoid–kyanite assemblages: eclogite facies indicators of subduction constraints in orogenic belts. *Journal of Metamorphic Geology* 28, 753–768.
- Söderlund, U., Patchett, P.J., Vervoort, J.D., Isachsen, C.E., 2004. The ^{176}Lu decay constant determined by Lu–Hf and U–Pb isotope systematics of Precambrian mafic intrusions. *Earth and Planetary Science Letters* 219, 311–324.
- Spandler, C., Hermann, J., Arculus, R., Mavrogenes, J., 2003. Redistribution of trace elements during prograde metamorphism from lawsonite blueschist to eclogite facies; implications for deep subduction zone processes. *Contributions to Mineralogy and Petrology* 146, 205–222.
- Spandler, C., Hermann, J., Arculus, R., Mavrogenes, J., 2004. Geochemical heterogeneity and element mobility in deeply subducted oceanic crust: insights from high-pressure mafic rocks from New Caledonia. *Chemical Geology* 206, 21–42.
- Stacey, J.S., Kramers, J.D., 1975. Approximation of terrestrial lead isotope evolution by a two stage model. *Earth and Planetary Science Letters* 26, 207–221.
- Sun, S.S., McDonough, W.F., 1989. Chemical and isotopic systematics of oceanic basalts: implications for mantle composition and processes. In: Saunders, A.D., Norry, M.J. (Eds.), *Magma-tism in the ocean basins*. Geological Society London Special Publications vol. 42, pp. 313–345.
- Sun, Z.M., Pei, J.L., Li, H.B., Xu, W., Jiang, W., Zhu, Z.M., Wang, X.S., Yang, Z.Y., 2012. Palaeomagnetism of late Cretaceous sediments from southern Tibet: Evidence for the consistent palaeolatitudes of the southern margin of Eurasia prior to the collision with India. *Gondwana Research* 21, 53–63.
- Tian, Z.L., Wei, C.J., 2014. Coexistence of garnet blueschist and eclogite in South Tianshan, NW China: dependence of P–T evolution and bulk-rock composition. *Journal of Metamorphic Geology* 32, 743–764.
- Turcotte, D.L., Schubert, G., 2002. *Geodynamics*. Cambridge University Press, New York (456 pp.).
- Van Orman, J.A., Grove, T.L., Shimizu, N., Layne, G.D., 2002. Rare earth element diffusion in a natural pyrope single crystal at 2.8 Ga. *Contributions to Mineralogy and Petrology* 142, 416–424.
- Vervoort, J.D., Patchett, P.J., Söderlund, U., Baker, M., 2004. Isotopic composition of Yb and the determination of Lu concentrations and Lu/Hf ratios by isotope dilution using MC-ICPMS. *Geochemistry, Geophysics, Geosystems* 5, Q11002. <http://dx.doi.org/10.1029/2004GC000721>.
- Wendt, I., Carl, C., 1991. The statistical distribution of the mean squared weighted deviation. *Chemical Geology* 86, 275–285.
- White, R.W., Powell, R., Holland, T.J.B., 2007. Progress relating to calculation of partial melting equilibria for metapelites. *Journal of Metamorphic Geology* 25, 511–527.
- White, R.W., Powell, R., Holland, T.J.B., Green, J., 2014. New mineral activity–composition relations for thermodynamic calculations in metapelitic systems. *Journal of Metamorphic Geology* 32, 261–286.
- Wijbrans, J.R., Pringle, M.S., Koppers, A.A.P., Scheveers, R., 1995. Argon geochronology of small samples using the Vulkan argon laser probe. *Proceedings of the Royal Netherlands Academy of Arts and Sciences* 98, 185–218.
- Xu, Z.Q., Zeng, L.S., Liu, F.L., Yang, J.S., Zhang, Z.M., McWilliams, M., Liou, J.G., 2006. Poly-phase subduction and exhumation of the Sulu high-pressure-ultra-high-pressure metamorphic terrane. *Geological Society of America, Special Paper* 403, 93–113.
- Xu, X.Z., Yang, J.S., Li, T.F., Chen, S.Y., Ren, Y.F., Li, Z.L., Shi, Y.R., 2007. SHRIMP U–Pb ages and inclusions of zircons from the Sumdo eclogite in the Lhasa block, Tibet, China. *Geological Bulletin of China* 26, 1340–1355.
- Xu, Q., Zhao, J.M., Yuan, X.H., Liu, H.B., Pei, S.P., 2015. Mapping crustal structure beneath southern Tibet: Seismic evidence for continental crustal under thrusting. *Gondwana Research* 27, 1487–1493.
- Yang, J.S., Xu, Z.Q., Geng, Q.R., Li, Z.L., Xu, X.Z., Li, T.F., Ren, Y.F., Li, H.Q., Cai, Z.H., Liang, F.H., Chen, S.Y., 2006. A possible new HP–UHP (?) metamorphic belt in China: discovery of eclogite in the Lhasa terrane Tibet. *Acta Geologica Sinica* 80, 1787–1792 (in Chinese with English abstract).
- Yang, J.S., Xu, Z.Q., Li, Z.L., Xu, X.Z., Li, T.F., Ren, Y.F., Li, H.Q., Chen, S.Y., Robinson, P.T., 2009. Discovery of an eclogite belt in the Lhasa block, Tibet: a new border for Paleo-Tethys? *Journal of Asian Earth Sciences* 34, 76–89.
- Yin, A., Harrison, T.M., 2000. Geologic evolution of the Himalayan Tibetan Orogen. *Annual Review of Earth and Planetary Sciences* 28, 211–280.
- Zeng, L.S., Liu, J., Gao, L.E., Chen, F.Y., Xie, K.J., 2009. Early Mesozoic high-pressure metamorphism within the Lhasa Block, Tibet and its implications for regional tectonics. *Earth Science Frontiers* 16, 140–151 (in Chinese with English abstract).
- Zhang, H.F., Xu, W.C., Guo, J.Q., Zong, K.Q., Cai, H.M., Yuan, H.L., 2007. Indosinian Orogenesis of the Gangdise Terrane: Evidences from Zircon U–Pb Dating and Petrogenesis of Granitoids. *Earth Science* 32, 155–166 (in Chinese with English abstract).
- Zhang, D.D., Zhang, L.F., Zhao, Z.D., 2011. A study of metamorphism of Sumdo eclogite in Tibet, China. *Earth Science Frontiers* 18, 116–126 (in Chinese with English abstract).
- Zhang, J.J., Santosh, M., Wang, X.X., Guo, L., Yang, X.Y., Zhang, B., 2012a. Tectonics of the northern Himalaya since the India–Asia collision. *Gondwana Research* 21, 939–960.
- Zhang, Z.M., Dong, X., Santosh, M., Liu, F., Wang, W., Yiu, F., He, Z.Y., Shen, K., 2012b. Petrology and geochronology of the Namche Barwa Complex in the eastern Himalayan syntaxis, Tibet: Constraints on the origin and evolution of the north–eastern margin of the Indian Craton. *Gondwana Research* 21, 123–137.
- Zhang, Y.C., Shi, G.R., Shen, S.Z., 2013. A review of Permian stratigraphy, palaeobiogeography and palaeogeography of the Qinghai–Tibet Plateau. *Gondwana Research* 24, 55–76.
- Zhang, X.R., Shi, R.D., Huang, Q.S., Liu, D.L., Gong, X.H., Chen, S.S., Wu, K., Yi, G.D., Sun, Y.L., Ding, L., 2014a. Early Jurassic high-pressure metamorphism of the Amdo terrane, Tibet: Constraints from zircon U–Pb geochronology of mafic granulites. *Gondwana Research* 26, 975–985.
- Zhang, Z.M., Dong, X., Santosh, M., Zhao, G.C., 2014b. Metamorphism and tectonic evolution of the Lhasa terrane, Central Tibet. *Gondwana Research* 25, 170–189.
- Zhao, J.M., Zhao, D.P., Zhang, H., Liu, H.B., Huang, Y., Cheng, H.G., Wang, W., 2014. P–wave tomography and dynamics of the crust and upper mantle beneath western Tibet. *Gondwana Research* 25, 1690–1699.
- Zheng, Y.-F., 2012. Metamorphic chemical geodynamics in continental subduction zones. *Chemical Geology* 328, 5–48.
- Zhu, D.C., Zhao, Z.D., Niu, Y.L., Dilek, Y., Wang, L.Q., Mo, X.X., 2011. Lhasa Terrane in southern Tibet came from Australia. *Geology* 39, 727–730.
- Zhu, D.C., Zhao, Z.D., Niu, Y.L., Dilek, Y., Hou, Z.Q., Mo, X.X., 2013. The origin and pre-Cenozoic evolution of the Tibetan Plateau. *Gondwana Research* 23, 1429–1454.